INL/JOU-21-65126-Revision-0

# Accelerated statistical failure analysis of multifidelity TRISO fuel models

February 2022

Changing the World's Energy Future

Som LakshmiNarasimha Dhulipala, Wen Jiang, Benjamin W Spencer, Jason D Hales, Michael D Shields, Andrew E Slaughter, Zachary M Prince, Chandrakanth Bolisetti, Vincent M Laboure, Promit Chakraborty

Idaho National Laboratory

INL is a U.S. Department of Energy National Laboratory operated by Battelle Energy Alliance, LLC

**DISCLAIMER**

This information was prepared as an account of work sponsored by an agency of the U.S. Government. Neither the U.S. Government nor any agency thereof, nor any of their employees, makes any warranty, expressed or implied, or assumes any legal liability or responsibility for the accuracy, completeness, or usefulness, of any information, apparatus, product, or process disclosed, or represents that its use would not infringe privately owned rights. References herein to any specific commercial product, process, or service by trade name, trade mark, manufacturer, or otherwise, does not necessarily constitute or imply its endorsement, recommendation, or favoring by the U.S. Government or any agency thereof. The views and opinions of authors expressed herein do not necessarily state or reflect those of the U.S. Government or any agency thereof.

INL/JOU-21-65126-Revision-0

# Accelerated statistical failure analysis of multifidelity TRISO fuel models

**Som LakshmiNarasimha Dhulipala, Wen Jiang, Benjamin W Spencer, Jason D Hales, Michael D Shields, Andrew E Slaughter, Zachary M Prince, Chandrakanth Bolisetti, Vincent M Laboure, Promit Chakraborty**

**February 2022**

**Idaho National Laboratory**
**Idaho Falls, Idaho 83415**

**http://www.inl.gov**

**Prepared for the**
**U.S. Department of Energy**
**Under DOE Idaho Operations Office**
**Contract DE-AC07-05ID14517**

# Accelerated Statistical Failure Analysis of Multifidelity TRISO Fuel Models

Somayajulu L. N. Dhulipala[a,*], Wen Jiang[a], Benjamin W. Spencer[a], Jason D. Hales[a], Michael D. Shields[b], Andrew E. Slaughter[c], Zachary M. Prince[d], Vincent M. Labouré[d], Chandrakanth Bolisetti[e], Promit Chakroborty[b]

[a] *Computational Mechanics and Materials, Idaho National Laboratory, Idaho Falls, ID 83402, USA*
[b] *Department of Civil and Systems Engineering, Johns Hopkins University, Baltimore, MD 21218, USA*
[c] *Computational Frameworks, Idaho National Laboratory, Idaho Falls, ID 83402, USA*
[d] *Reactor Physics Methods and Analysis, Idaho National Laboratory, Idaho Falls, ID 83402, USA*
[e] *Advanced Reactor Technology and Design, Idaho National Laboratory, Idaho Falls, ID 83402, USA*

**Abstract**

Statistical nuclear fuel failure analysis is critical for the design and development of advanced reactor technologies. Although Monte Carlo Sampling (MCS) is a standard method of statistical failure analysis for fuels, the low failure probabilities of some advanced fuel forms and the correspondingly large number of required model evaluations limit its application to low-fidelity (e.g., 1-D) fuel models. In this paper, we present four other statistical methods for fuel failure analysis in Bison, considering tri-structural isotropic (TRISO)-coated particle fuel as a case study. The statistical methods considered are Latin hypercube sampling (LHS), adaptive importance sampling (AIS), subset simulation (SS), and the Weibull theory. Using these methods, we analyzed both 1-D and 2-D representations of TRISO models to compute failure probabilities and the distributions of fuel properties that result in failures. The results of these methods compare well across all TRISO models considered. Overall, SS and the Weibull theory were deemed the most efficient, and can be applied to both 1-D and 2-D TRISO models to compute failure probabilities. Moreover, since SS also characterizes the distribution of parameters that cause TRISO failures, and can consider failure modes not described by the Weibull criterion, it may be preferred over the other methods. Finally, a discussion on the efficacy of different statistical methods of assessing nuclear fuel safety is provided.

*Keywords:* Monte Carlo; Variance Reduction; Bison; Nuclear Fuel; Risk; Reliability

## 1. Introduction

In many advanced reactor concepts currently under consideration (e.g., high-temperature gas-cooled reactors and fluoride-salt-cooled high-temperature reactors), the reliability of nuclear fuel in preventing fission product release into the coolant is critical from both operational and safety perspectives [4]. As such, several recent studies have assessed not only the safety of advanced reactor fuels [22, 3], but also the consequences of fuel failure to the overall safety of nuclear plants [23]. There has also been interest in improving the modeling fidelity of computational fuel models for enhanced accuracy and robustness [8, 6]. Failure assessment of nuclear fuels consists of a combination of (1) experiments to provide data for specific conditions, (2) computational modeling, which is validated against the available data, and (3) uncertainty quantification (UQ) to account for randomness in fuel properties and operating conditions. Once the parameters of the computational model are calibrated, the quality and computational feasibility of failure analysis depend on having a proper balance between the level of modeling fidelity and the efficiency of the UQ method. Standard UQ methods such as Monte Carlo Sampling (MCS) are expensive to run both in terms of the simulation time and computational resources, mostly permitting only the use of low-fidelity

*Corresponding author; Email: Som.Dhulipala@inl.gov

fuel models (e.g., 1-D models; see Jiang et al. [11] and Miller et al. [19]). Therefore, this paper presents alternative statistical methods made available in the Bison fuel performance code [30] (itself built on the Multiphysics Object-Oriented Simulation Environment [MOOSE] [24]) for failure analysis of nuclear fuels. Tri-structural isotropic (TRISO)-coated particle fuel was chosen as a case study for the present work, and some of the presented methods are able to consider both low- and high-fidelity models of the TRISO fuel for statistical failure analysis.

Due to its ability to contain fission products under even extreme operating temperatures, the use of TRISO particle fuel in advanced reactor technologies has generated a great deal of interest. As detailed in Williamson et al. [29] and Jiang et al. [12], each TRISO particle is composed of the fuel kernel, buffer, inner pyrolytic carbon (IPyC), silicon carbide (SiC), and outer pyrolytic carbon (OPyC) layers. This fuel is considered "failed" if the SiC layer fails [12], though the probability of failure is low, with values typically ranging from $1E-3$ to $1E-7$, depending on the fuel properties and irradiation conditions. The SiC layer failure is mostly caused due to the cracking of the IPyC layer resulting in stress concentration in the SiC layer, although other failure modes are also possible. From a modeling viewpoint, while the MCS approach is a standard and widely accepted method, it requires numerous evaluations of the TRISO model (on the order of hundreds of thousands to millions) to accurately calculate the failure probabilities [12, 19]. Thus, most TRISO failure studies have relied on 1-D approximations of the TRISO model, with the multidimensional stress state in the TRISO layers being approximated by a 1-D stress state [12, 19]. However, it is desirable to consider high-fidelity TRISO models (i.e., 2-D models) when performing failure analysis, and for this, statistical methods beyond MCS are necessary. Also, because of TRISO fuel's robustness and resulting very low probability of failure, its statistical analysis particularly stands to benefit from the more advanced methods studied here.

For failure analysis of TRISO fuel, we present four methods as alternatives to MCS. Figure 1 presents an overview of the uncertain input parameters of the TRISO model, multifidelity TRISO models, and statistical methods of failure analysis. Among these methods, Latin hypercube sampling (LHS), while more effectively partitioning the input parameter space than MCS, is considered a standard method. More advanced variance reduction methods such as adaptive importance sampling (AIS) and subset simulation (SS) reduce the uncertainty (as compared to MCS and LHS) in failure probability estimates for a given number of model evaluations by intelligently exploring the input space. The final method, referred to here as Weibull theory, is tied to the use of Weibull statistics [31] in defining the failure criterion for the PyC and SiC layers. The Weibull model directly provides a failure probability for a given sample, and the failure probability for a set of samples can be taken as the average of the failure probability from each of those samples. Failure analysis of TRISO fuel can be used both to accurately determine the failure probability and to characterize distributions of the input parameters that cause TRISO failure. While the former is important for ensuring fuel safety, the latter aids in optimizing fuel design and fabrication [7].

We consider four 1-D models of TRISO fuel with varying characteristics and operating conditions, then apply the five statistical analysis methods in Figure 1 to compute outcomes such as failure probabilities and the distributions of parameters that cause model failures. We compare the five methods in terms of their accuracy and efficiency in simulating these results. Next, we consider 2-D versions of the four TRISO models to compute the failure probabilities and parameter distributions when using SS and the Weibull theory. We not only compare the results from the SS and Weibull theory with each other, but also compare the 2-D results with the corresponding 1-D results for these two methods. Note that the other three methods are too computationally prohibitive for use with 2-D TRISO models. Since the statistical methods presented in Figure 1 do not all have the same efficacy and capabilities for fuel safety analysis, a discussion on this is also provided.

This paper is organized as follows. Section 2 provides background on TRISO fuel modeling in Bison by discussing the thermo-mechanical properties, fuel failure modes, and considered TRISO models. Section 3 presents the algorithmic details of the five statistical methods listed in Figure 1. Section 4 discusses the 1-D TRISO model results for failure probabilities and input parameter distributions of failed TRISO particles. Section 5 discusses these results for 2-D TRISO models. Section 6 discusses the efficacy of the different statistical methods. Finally, Section 7 summarizes this paper and presents its conclusions.

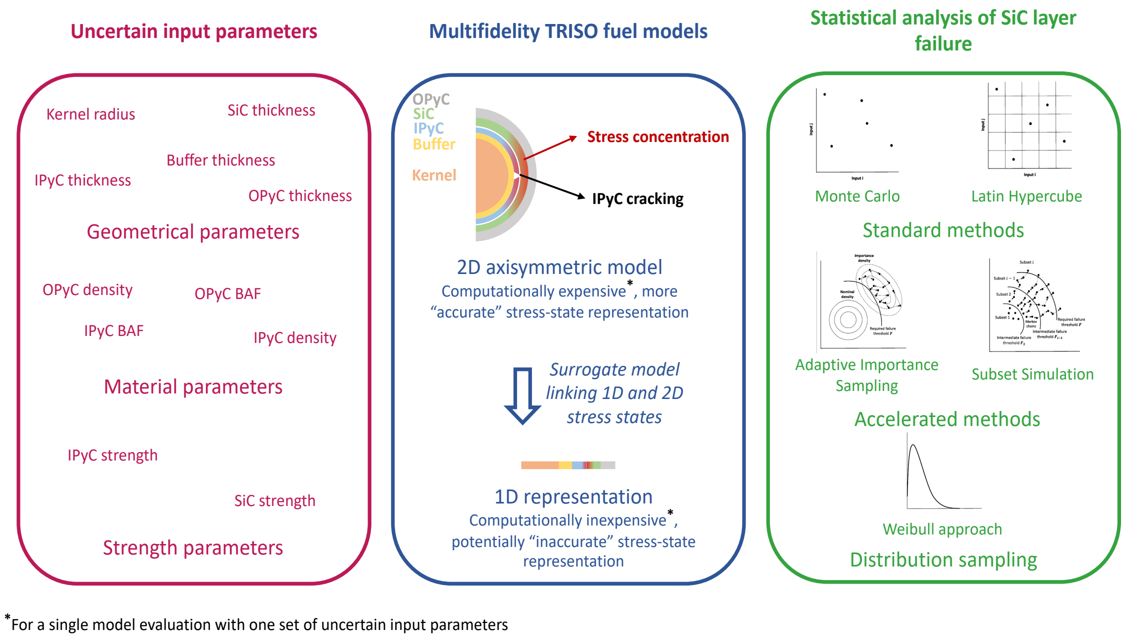


Figure 1: Overview of the uncertain input parameters of the TRISO model, multifidelity TRISO models, and statistical methods for failure analysis. (**Abbreviations** IPyC: inner pyrolytic carbon; SiC: silicon carbide; OPyC: outer pyrolytic carbon; and BAF: Bacon Anisotropy Factor)

## 2. Background on TRISO modeling with Bison and the models considered

### 2.1. Governing equations

As detailed in Jiang et al. [12] and Williamson et al. [29], fuel simulations are generally governed by two equations: heat and momentum conservation. The heat equation is given by:

$$\rho \, C_p \, \frac{\partial T}{\partial t} + \nabla \cdot (-k \nabla T) - E_f \, \dot{F} = 0 \tag{1}$$

where $T$ is the unknown temperature and $k$, $C_p$, $\rho$, $E_f$, and $\dot{F}$ are the thermal conductivity, specific heat, density, energy released per fission, and volumetric fission rate, respectively. The momentum conservation equation (neglecting body forces) is given by:

$$\nabla \cdot \boldsymbol{\sigma} = 0 \tag{2}$$

where $\boldsymbol{\sigma}$ is the Cauchy stress tensor. The constitutive law (assuming small strains) is given by:

$$\boldsymbol{\sigma} = \mathcal{C} : (\boldsymbol{\varepsilon} - \boldsymbol{\varepsilon}_c - \boldsymbol{\varepsilon}_t - \boldsymbol{\varepsilon}_i) \tag{3}$$

where $\mathcal{C}$ is the elasticity tensor and $\boldsymbol{\varepsilon}$, $\boldsymbol{\varepsilon}_c$, $\boldsymbol{\varepsilon}_t$, and $\boldsymbol{\varepsilon}_i$ are the total strain, irradiation creep strain, thermal expansion strain, and irradiation-induced eigenstrain, respectively.

### 2.2. Thermo-mechanical properties

The thermo-mechanical behavior of each TRISO particle layer (i.e., the fuel kernel, buffer, IPyC, SiC, and OPyC) depends on a number of properties. Thermal conductivity, specific heat, thermal expansion, Young's modulus, and Poisson's ratio are among these important properties, and Table 1 gives a brief overview of these properties for each layer. Modeling of a TRISO particle also depends on parameters and properties not included in Table 1. Furthermore, some of the properties in Table 1 themselves depend on other material properties. For example, the molar mass of the fuel kernel depends on the initial U-235 enrichment, initial oxygen-to-uranium and carbon-to-uranium stoichiometries, etc. The irradiation-creep-induced deformation of the buffer and IPyC/OPyC layers, which is proportional to the fast neutron fluence, depends on the steady-state creep coefficient. The buffer also experiences an isotropic irradiation-induced strain modeled as a quartic polynomial function whose coefficients depend on temperature. Under irradiation, IPyC/OPyC layers experience strains in both the tangential and radial directions, and these are modeled as a quartic polynomial function whose coefficients depend on both the temperature and Bacon anisotropy factor (BAF). Jiang et al. [12] provides a more exhaustive description of the thermo-mechanical properties that must be considered when modeling a TRISO particle.

Table 1: Summary of the thermo-mechanical properties used in the TRISO model.

| | **Fuel kernel** | **Buffer layer** | **IPyC/OPyC layers** | **SiC layer** |
|---|---|---|---|---|
| **Thermal conductivity** $k$ $(W/K/m)$ | $0.0132\ \exp(0.00188T_C)$ $+\frac{4040}{464+T_C}\ H(T_C-1650)$ $+1.9-1.9\ H(T_C-1650)$ | $\frac{x}{y}$ <br> $x=k_{in}k_{th}\rho_{th}$ $(\rho_{th}-\rho_{in})$ <br> $y=k_{th}\rho_{th}(\rho_{th}-\rho)$ $+k_{in}\rho(\rho-\rho_{in})$ | 4 | $\frac{17885}{T_K}+2.0$ |
| **Specific heat** $C_p$ $(J/K/kg)$ | $\frac{1}{M}\big(52.1743+87.951\ t_K$ $-84.2411\ t_K^2+31.542\ t_K^3$ $-2.6334\ t_K^4+\frac{0.71391}{t_K^2}\big)$ | 720 | 720 | $925.65+0.377T_K$ $-7.926E-5\ T_K^2$ $-3.194E+7\ T_K^{-2}$ |
| **Thermal expansion** $\alpha$ $(1/K)$ | — | $5\big(1+0.11$ $\frac{T_C-400}{700}\big)$ | $1E-6\ \alpha_i$ <br> $i=$ radial $(30-37.5R_r)$ $\big(1+0.11[\frac{T_K-673}{700}]\big)$ <br> $i=$ tangential $(36[R_t-1]^2+1)$ $\big(1+0.11[\frac{T_K-673}{700}]\big)$ | $4.9E-6$ |
| **Young's modulus** $E$ $(GPa)$ | $219\big(1.0-1.1E-4\ T_C$ $-2.1E-7\ T_C^2$ $+3.1E-10\ T_C^3$ $-1.6E-13\ T_C^4\big)$ $\frac{1.92\rho-0.92\rho_{th}}{\rho_{th}}$ | $25.5(0.384+$ $0.324E-3\ \rho)$ $(1+0.23\phi)$ $(1+1.51E-4$ $[T_C-20])$ | $(E_r+E_t)/2$ | 428 ($T_C<25^o$C) <br> Linear interpolation [19] ($25^o$C $<T_C<1600^o$C) <br> 198 ($T_C>1600^o$C) |
| **Poisson's ratio** $\nu$ | $1.35\left(\frac{1.92\rho-0.92\rho_{th}}{1.66\rho-0.66\rho_{th}}\right)-1$ | 0.33 <br> 0.5 (creep) | 0.33 <br> 0.5 (creep) | 0.13 |

**Notations**. $T_C$: temperature in $^o$C; $T_K$: temperature in K; $t_K$ : $T_K/1000$; $\rho$: density; $\rho_{th}$: theoretical density; $\rho_{in}$: initial density; $k$: thermal conductivity; $k_{th}$: theoretical thermal conductivity; $k_{in}$: initial thermal conductivity; $E_r$ and $E_t$: radial and tangential components of the Young's modulus; $R_r$ and $R_t$: radial and tangential components of orientation parameter; $\phi$: fast neutron flux; and $M$: molar mass of the kernel

### *2.3. Failure characterization using multifidelity models*

Three failure modes for TRISO particles are considered here [12]:

1. *Pressure vessel failure of a spherical particle*: While the PyC layers shrink, causing compressive stresses in the SiC during the initial irradiation, the creep in the PyC layers eases this compression. SiC failure

occurs when the maximum tangential tensile stress exceeds the SiC strength. Gas pressure buildup in the buffer and IPyC gap can also lead to tensile stresses in the SiC. However, this failure mode is not likely to occur in an intact particle at low or intermediate temperatures for the UCO fuel kernel.
2. *IPyC cracking*: Shrinking of the IPyC layer during irradiation can cause the tensile stress to exceed the IPyC strength and result in IPyC cracking. As presented in Figure 2, once the IPyC cracks, the SiC layer experiences a significant degree of stress concentration. If the tangential tensile stress in the SiC exceeds the SiC strength, this can lead to TRISO particle failure.
3. *Pressure vessel failure of an aspherical particle*: Fabrication defects in the TRISO particle can lead to asphericity, potentially exacerbating the effects of the PyC layer shrinkage and the fission gas buildup in the fuel kernel. These effects could cause the tangential tensile stresses in the SiC to exceed its strength.

In addition to the three failure modes described above, other failure modes such as layer debonding [17] are also possible and could contribute to TRISO particle failure. Modeling of additional failure modes using Bison is being actively investigated.

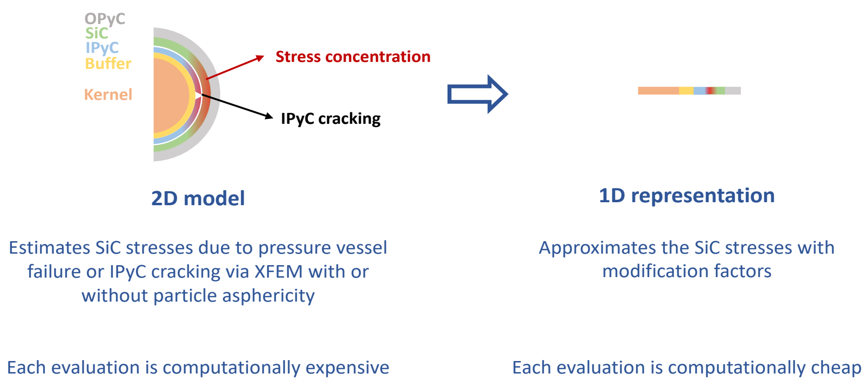


Figure 2: 1-D and 2-D representations of the TRISO model. While the 2-D model can directly account for SiC stresses due to IPyC cracking and pressure vessel failure, the 1-D model indirectly considers such aspects by using stress modification factors.

The IPyC and SiC layers are considered failed when the maximum tensile stress exceeds their strength. A Weibull distribution is used for modeling the layer strength ($\sigma_s$) [12]:

$$\sigma_s \sim \mathcal{W}(\sigma_{ms},\ m) = \frac{m}{\sigma_{ms}}\left(\frac{\sigma_s}{\sigma_{ms}}\right)^{m-1} \exp\left(-\frac{\sigma_s}{\sigma_{ms}}\right)^{m} \tag{4}$$

where $\sigma_{ms}$ is the mean strength, which depends on the characteristic strength [12], and $m$ is the Weibull modulus (9.5 and 6 for the IPyC and SiC, respectively).

Analysis of some of the failure modes in TRISO fuel involves the modeling of particle asphericity and cracks in the IPyC layer, thus requiring a 2-D model. Standard methods such as MCS or LHS require hundreds of thousands to millions of evaluations of the TRISO model to accurately estimate the failure probability. Numerous model evaluations using the 2-D model can be infeasible, even with parallel computing. Thus, fast-running 1-D approximations of the 2-D model were developed for the PARFUME code [19], and also adopted by Jiang et al. [12] in Bison. As presented in Figure 2, to appropriately account for phenomena such as stress concentrations in SiC as well as SiC stresses due to particle asphericity, stress modification factors were used to modify the stresses from the 1-D model. The modification factor for the SiC stress concentration due to IPyC cracking is [12]:

$$\sigma_{IPyC\_crack} = \frac{\bar{\sigma}_{2D}}{\bar{\sigma}_{1D}}\ \sigma_{1D} \tag{5}$$

where $\bar{\sigma}_{2D}$ and $\bar{\sigma}_{1D}$ are the maximum mean stresses in the 2-D and 1-D models, respectively, and $\sigma_{1D}$ is the stress in the 1-D model. The modification factor for SiC stress due to particle asphericity is [12]:

$$\sigma_{asphericity} = \frac{\bar{\sigma}_{2D}}{\bar{\sigma}_{1D}}\ \sigma_{1D\_min} + \frac{\Delta\bar{\sigma}_{2D}}{\Delta\bar{\sigma}_{1D}}\ \Delta\sigma_{1D\_min} \tag{6}$$

where $\Delta\bar{\sigma}_{2D}$, $\Delta\bar{\sigma}_{1D}$, and $\Delta\sigma_{1D\_min}$ represent changes in stresses $\sigma_{2D}$, $\sigma_{1D}$, and $\sigma_{1D\_min}$, respectively, going from the beginning to the end of irradiation. The factors $\frac{\bar{\sigma}_{2D}}{\bar{\sigma}_{1D}}$ and $\frac{\Delta\bar{\sigma}_{2D}}{\Delta\bar{\sigma}_{1D}}$ for the TRISO models considered in this study are presented next. Note that, in this study, both the 2-D model and 1-D approximation are used to characterize TRISO failure. Also, both the 2D and 1D TRISO models have the same failure modes.

### *2.4. TRISO models considered*

We consider four TRISO models studied by Jiang et al. [12] for which a variety of characteristics and operating conditions are explored. These four models mainly differ in terms of their randomized input parameters, input parameter distributions, fuel characteristics, and irradiation temperatures. Table 2 presents the input parameters for the four TRISO models considered. Models 1 and 2 correspond to the Advanced Gas Reactor (AGR)-2 experiment compacts 5-1-3 and 5-3-3, respectively, from the study by Jiang et al. [12]. Models 3 and 4 correspond to the benchmark verification cases with PARFUME under conditions 1 and 2, respectively, from the study by Jiang et al. [12]. In line with Jiang et al. [12], it is noted that, while Models 1 and 2 have seven random parameters, Models 3 and 4 have eleven. Additionally, the irradiation temperatures across the four models are also different. These temperatures for Models 1 and 2 depend on the fluence value which changes on a daily basis and have [minimum, maximum] values of [207.4$^o$C, 1226.84$^o$C] and [195.84$^o$C, 1281.84$^o$C], respectively. For Models 3 and 4, the constant irradiation temperatures are 700.0$^o$C and 1000.0$^o$C, respectively. Figure 3 presents the time versus temperature and fluence versus temperature plots for models 1 and 2 which have variable temperatures.

Table 2: Input parameters for the four TRISO models considered in this study. Models 1 and 2 correspond to the AGR-2 experiment compacts 5-1-3 and 5-3-3, respectively. Models 3 and 4 correspond to benchmark verification cases with PARFUME. These parameters and the corresponding distributions (if any) were obtained from the study by Jiang et al. [12].

| **Category** | **Parameter** | **Models 1 & 2** | **Models 3 & 4** |
|---|---|---|---|
| Fuel characteristics | $^{235}$U enrichment (wt %) | 14.029 | 15.5 |
| | Carbon/Uranium (atomic ratio) | 0.392 | 0.4 |
| | Oxygen/Uranium (atomic ratio) | 1.428 | 1.5 |
| Particle geometry | Kernel radius ($\mu m$) | $\mathcal{N}(213.35,\ 4.4)$ | $\mathcal{N}(212.5,\ 5.0)$ |
| | Buffer thickness ($\mu m$) | $\mathcal{N}(98.9,\ 8.4)$ | $\mathcal{N}(100.0,\ 10.0)$ |
| | IPyC thickness ($\mu m$) | $\mathcal{N}(40.4,\ 2.5)$ | $\mathcal{N}(40.0,\ 3.0)$ |
| | SiC thickness ($\mu m$) | $\mathcal{N}(35.2,\ 1.2)$ | $\mathcal{N}(35.0,\ 2.0)$ |
| | OPyC thickness ($\mu m$) | $\mathcal{N}(43.4,\ 2.9)$ | $\mathcal{N}(40.0,\ 3.0)$ |
| | Asphericity | 1.0 | 1.04 |
| Fuel properties | Kernel density ($g/cm^3$) | 10.966 | 11.0 |
| | Kernel theoretical density ($g/cm^3$) | 11.37 | 11.4 |
| | Buffer density ($g/cm^3$) | 1.05 | 1.05 |
| | Buffer theoretical density ($g/cm^3$) | 2.25 | 2.25 |
| | IPyC density ($g/cm^3$) | 1.89 | $\mathcal{N}(1.9,\ 0.02)$ |
| | OPyC density ($g/cm^3$) | 1.907 | $\mathcal{N}(1.9,\ 0.02)$ |
| | IPyC BAF | 1.0465 | $\mathcal{N}(1.05,\ 0.005)$ |
| | OPyC BAF | 1.0429 | $\mathcal{N}(1.05,\ 0.005)$ |
| Layer strengths | IPyC | $\mathcal{W}(\sigma_{ms},\ 9.5)$ | $\mathcal{W}(\sigma_{ms},\ 9.5)$ |
| | SiC | $\mathcal{W}(\sigma_{ms},\ 6.0)$ | $\mathcal{W}(\sigma_{ms},\ 6.0)$ |

**Notations:** $\mathcal{N}(x,\ y)$: normal distribution with mean $x$ and standard deviation $y$; $\sigma_{ms}$: mean strength, which is dependent on the characteristic strength obtained from Jiang et al. [12]; $\mathcal{W}(\sigma_{ms},\ m)$: Weibull distribution with mean strength $\sigma_{ms}$ and Weibull modulus $m$.

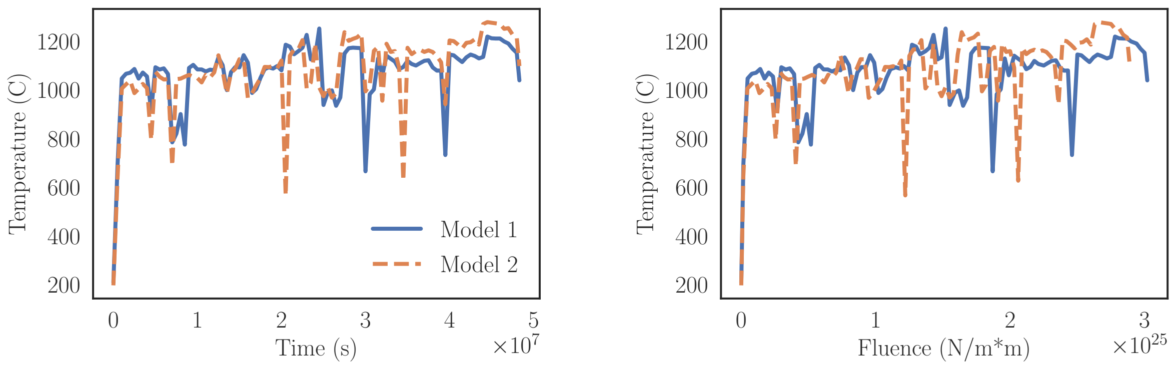


(a) (b)

Figure 3: (a) Time versus temperature plot and (b) fluence versus temperature plot for models 1 and 2.

For the 1-D TRISO models, the stress modification factors described in Equations (5) and (6) also differ for each of the four considered models. Table 3 presents these modification factors for both IPyC cracking and particle asphericity. These stress modification factors are obtained from Jiang et al. [12] who used a regular Monte Carlo simulation to compute TRISO failure probabilities considering 1D models.

Table 3: Stress modification factors for the 1-D models obtained from Jiang et al. [12]

| **Modification factor** | **Model 1** | **Model 2** | **Model 3** | **Model 4** |
|---|---|---|---|---|
| IPyC cracking $\frac{\bar{\sigma}_{2D}}{\bar{\sigma}_{1D}}$ | -1.19 | -1.239 | -0.87 | -0.97 |
| Asphericity $\frac{\bar{\sigma}_{2D}}{\bar{\sigma}_{1D}}$ | 1.39 | 1.41 | 1.41 | 1.59 |
| Asphericity $\frac{\Delta\bar{\sigma}_{2D}}{\Delta\bar{\sigma}_{1D}}$ | 1.21 | 1.24 | 1.22 | 1.41 |

## 3. Description of the statistical methods for fuel failure analysis

For estimating the TRISO failure probability, we are interested in computing the following integral:

$$P_f = \int_{F(\boldsymbol{x}) \geq \mathcal{F}} q(\boldsymbol{x})\ d\boldsymbol{x} \tag{7}$$

where $P_f$ is the failure probability, $q(\boldsymbol{x})$ is the joint distribution of the input parameters (which are the product of the distributions presented in Table 2, due to the lack of input parameter correlations), and $F(\boldsymbol{x}) \geq \mathcal{F}$ represents the TRISO particle failure criterion. Herein, the TRISO particle is considered to have failed if the SiC stress exceeds the SiC strength which is likely caused due to IPyC cracking resulting in stress concentrations in the SiC layer, as discussed in Section 2.3. As such, in Equation (7), $F(\boldsymbol{x})$ corresponds to the difference between the SiC stress and strength, and the failure threshold $\mathcal{F}$ is set to zero. Along with the failure probability value, we are interested in the distribution of input parameters that cause TRISO particle failures. This distribution is defined as $q(\boldsymbol{x} \mid F(\boldsymbol{x}) \geq \mathcal{F})$ and is important for optimizing the fuel design and fabrication [7]. A number of Monte-Carlo-type methods are presented below for estimating both the failure probability and $q(\boldsymbol{x} \mid F(\boldsymbol{x}) \geq \mathcal{F})$.

### *3.1. Standard method: Monte Carlo Sampling*

In a MCS simulation, numerous sets of TRISO input parameters are randomly and independently drawn from appropriate distributions. The TRISO model is then independently evaluated for each set of input parameters. The TRISO failure probability is computed based on the outcomes of those evaluations as [16]:

$$\hat{P}_f^{\text{MCS}} = \frac{1}{N} \sum_{i=1}^{N} I\big(F(\boldsymbol{x}_i) \geq \mathcal{F}\big) \tag{8}$$

where $\hat{P}_f^{\text{MCS}}$ is the failure probability estimator computed via MCS, $N$ is the total number of TRISO model evaluations, $\boldsymbol{x}_i$ is a random set of TRISO input parameters, $F(\boldsymbol{x}_i) \geq \mathcal{F}$ represents the failure criterion for the $i^{\text{th}}$ model evaluation (i.e., $F(\boldsymbol{x}_i)$), and $I(.)$ is an indicator function for the TRISO model failure criterion. This indicator function is taken to be one if the failure criterion is met, and zero otherwise. The accuracy of the TRISO failure probability calculations is influenced by the number of TRISO model evaluations ($N$) relative to the magnitude of $\hat{P}_f^{\text{MCS}}$. A higher $N$ results in a more accurate estimate of this failure probability when using MCS. Likewise, the higher the true failure probability value, the greater the average accuracy in estimating it via MCS. Note that the true failure probability is not known in advance and that the estimator $\hat{P}_f^{\text{MCS}}$ converges to the true value as $N \to \infty$ [16].

Since $N$ is a finite (albeit large) value for practical applications, and because TRISO fuel failure evaluation is safety-critical, a measure of the accuracy of the failure probability estimate should always be specified along with the failure probability estimate itself. This measure of accuracy is termed the coefficient of variation (COV) and is derived using the variance estimate of $\hat{P}_f^{\text{MCS}}$ [16]:

$$\text{Var}(\hat{P}_f^{\text{MCS}}) = \frac{\hat{P}_f^{\text{MCS}}(1 - \hat{P}_f^{\text{MCS}})}{N} \tag{9}$$

where $\text{Var}(\hat{P}_f^{\text{MCS}})$ is the variance estimator over the failure probability estimate. Now, COV (denoted by $\hat{\delta}$) is defined as the ratio of square root of $\text{Var}(\hat{P}_f^{\text{MCS}})$ to $\hat{P}_f^{\text{MCS}}$:

$$\hat{\delta}^{\text{MCS}} = \frac{\sqrt{\text{Var}(\hat{P}_f^{\text{MCS}})}}{\hat{P}_f^{\text{MCS}}} = \sqrt{\frac{1 - \hat{P}_f^{\text{MCS}}}{\hat{P}_f^{\text{MCS}}\, N}} \tag{10}$$

As expected, the smaller the COV value, the greater the accuracy in estimating the failure probability (on average). Figure 4 presents a histogram of these failure probability estimates for each COV value. The lower the COV value, the narrower the histogram's spread of failure probability estimates. As the COV tends toward zero, the two independent evaluations of the failure probability will produce the exact same results; namely, the true value. However, with a reducing COV, the number of TRISO model evaluations will increase dramatically. COVs of 0.1 and 0.01 require $\sim 1E6$ and $\sim 1E8$ TRISO evaluations, respectively, if the true failure probability is $1E-4$. The number of required TRISO evaluations $N$ for a target failure probability and COV can be computed using Equation (10).

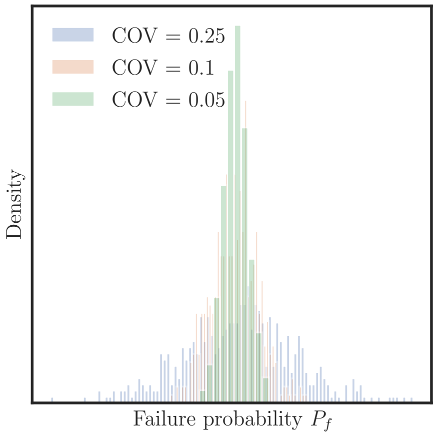


Figure 4: The COV's influence on the variability of the failure probability estimates. A smaller COV leads to more confidence in the failure probability.

A benefit of using MCS is that the TRISO model evaluations can be run in parallel, since they are independent of each other. For example, when using 1,000 processors for a target COV of 0.1 and a failure probability of $1E-4$, each processor only runs $1E3$ TRISO evaluations—as compared to $1E6$ evaluations when using serial computing. For a target COV of 0.01, each processor runs $1E5$ TRISO evaluations, as compared to $1E8$ evaluations in serial. Section 3.4 discusses parallel computing in Monte Carlo simulations in more depth in the context of the parallel SS method.

### *3.2. Standard method: Latin hypercube sampling*

Drawing the input parameters completely at random using MCS sampling can result in the input samples being clustered and some parts of the parameter space being inadequately explored when taking into consideration the finite number of samples drawn and the corresponding model evaluations performed due to computational budget limitations [21]. To some extent, LHS mitigates this clustering issue and improves the confidence over the failure probability estimate for a given number of TRISO evaluations ($N$), as compared to MCS (although for low failure probability values, this improvement is insignificant [20]). In LHS, if $n$ is the number of random input parameters, an $n$-dimensional cube (i.e., a hypercube) bounded between [0, 1] is first created. Each dimension of this hypercube is equally divided into $N$ partitions (the required number of TRISO evaluations). For example, as presented in Figure 5, if $n = 2$ and $N = 5$, a 2-D hypercube (i.e., a square) is created, with each side equally partitioned into five. The goal is for one—and only one—sample in each partition to correspond to an input dimension. Therefore, for a given sample and input dimension, the partition index is assigned randomly, without replacement. Partition indices corresponding to different input dimensions are randomly combined to define the location of a sample in the hypercube space; that is, the location of a sample is characterized by the cell location. In terms of the simple example in Figure 5, this means that each row and column will have only one sample, and that the row and column combinations are randomly assigned, without replacement. Once the location of a sample in the hypercube is defined via the cell location, the position of the sample within this cell can be either at the center (as in Figure 5) or randomly chosen. The final step in the LHS process is to transform the input sample from the hypercube space bounded between [0, 1] to that of the input parameters. This means transforming the location of a sample along an input dimension $j$ (i.e., $U_j$) to its probability distribution space $q(x_j)$. This transformation is accomplished using $x_j = Q^{-1}(U_j)$, where $Q^{-1}(.)$ is the inverse cumulative distribution function (CDF).

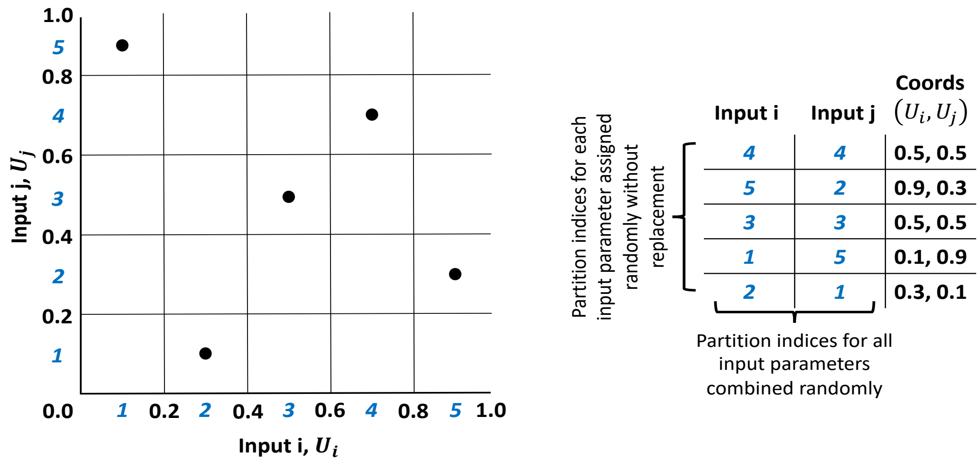


Figure 5: Partitioning scheme in LHS, illustrated for a 2-D parameter space for five samples. Partition indices are shown in blue, while probabilities are shown in black.

Once $N$ Latin hypercube samples are generated and the corresponding TRISO model evaluations are made, the failure probability is estimated in a fashion identical to MCS [15, 26]:

$$\hat{P}_f^{\text{LHS}} = \frac{1}{N} \sum_{i=1}^{N} I\big(F_i(\boldsymbol{x}) \geq \mathcal{F}\big) \tag{11}$$

The variance estimate of $\hat{P}_f^{\text{LHS}}$ is composed of two terms [15, 26]:

$$\begin{aligned} \text{Var}(\hat{P}_f^{\text{LHS}}) &= \text{Var}_1(\hat{P}_f^{\text{LHS}}) \qquad + \text{Var}_2(\hat{P}_f^{\text{LHS}}) \\ &= \frac{\hat{P}_f^{\text{LHS}}(1-\hat{P}_f^{\text{LHS}})}{N} + \frac{N-1}{N}\, \frac{1}{N^n\;(N-1)^n} \sum_R \left(\hat{\mu_i} - \hat{P}_f^{\text{LHS}}\right) \left(\hat{\mu_j} - \hat{P}_f^{\text{LHS}}\right) \end{aligned} \tag{12}$$

where $\hat{\mu_i}$ is the mean value of cell $i$ and $R$ denotes the $N^n\;(N-1)^n$ cell combinations with no common cell locations. The first variance term, $\text{Var}_1(\hat{P}_f^{\text{LHS}})$, is the same as that of MCS, and the second variance term, $\text{Var}_2(\hat{P}_f^{\text{LHS}})$, is referred to as the cell covariance. The LHS variance estimate would only be smaller than a MCS variance for $N$ samples when $\text{Var}_2(\hat{P}_f^{\text{LHS}})$ is negative. However, for small failure probabilities, the reduction in total variance $\text{Var}(\hat{P}_f^{\text{LHS}})$ is insignificant compared to that of MCS [20]. Thus, the COV can be approximated as:

$$\delta^{\text{LHS}} = \frac{\sqrt{\text{Var}(\hat{P}_f^{\text{LHS}})}}{\hat{P}_f^{\text{LHS}}} \approx \sqrt{\frac{1-\hat{P}_f^{\text{LHS}}}{\hat{P}_f^{\text{LHS}}\;N}} \tag{13}$$

which is the same as a MCS estimate for COV. As with MCS, LHS can be accelerated via parallel computing by first setting up the Latin hypercube samples and then evaluating the TRISO model for the input samples by using several processors simultaneously.

*3.3. Variance reduction method: adaptive importance sampling*

Both MCS and LHS require a large number of TRISO model evaluations to estimate the TRISO failure probability. Using more advanced variance reduction methods, it is possible to significantly reduce the number of model evaluations. For a given number of model evaluations, variance reduction methods can greatly decrease the amount of variance (and hence the COV) over the failure probability estimate, as compared to either MCS or LHS. Importance sampling is one such classical variance reduction method. In importance sampling, the definition of the failure probability is rewritten as [25]:

$$P_f^{\text{AIS}} = \int_{F(\boldsymbol{x}) \geq \mathcal{F}} \frac{q(\boldsymbol{x})\ f(\boldsymbol{x})}{f(\boldsymbol{x})}\ d\boldsymbol{x} \tag{14}$$

where $f(\boldsymbol{x})$ is termed the importance density. Equation (14) is equivalent to the failure probability definition in Equation (7). Due to the presence of the importance density $f(\boldsymbol{x})$, the statistical estimator for the failure probability is [25]:

$$\hat{P}_f^{\text{AIS}} = \frac{1}{N} \sum_{i=1}^{N} I\big(F_i(\boldsymbol{x}) \geq \mathcal{F}\big)\ \frac{q(\boldsymbol{x})}{f(\boldsymbol{x})} \tag{15}$$

If the importance density $f(\boldsymbol{x})$ is chosen appropriately, the failure probability can be estimated with more confidence and by using significantly fewer TRISO model evaluations than when applying either MCS or LHS. An appropriate choice of $f(\boldsymbol{x})$ can be [1]:

$$f(\boldsymbol{x}) \propto [I\big(F_i(\boldsymbol{x}) \geq \mathcal{F}\big) = 1]\ q(\boldsymbol{x}) \tag{16}$$

meaning that it is preferable for $f(\boldsymbol{x})$ to have a high probability density in the region of input parameter space where the TRISO model fails. Since identifying such a region of the parameter space can be difficult, an adaptive approach for constructing the importance density can be used. In this paper, the method of adaptive importance sampling (AIS) proposed by Au and Beck [1] is used. We first sample from the conditional distribution $q\Big(\boldsymbol{x}\Big|I\big(F_i(\boldsymbol{x}) \geq \mathcal{F}\big) = 1\Big)$ (i.e., the distribution of the input parameters that cause TRISO model failure) using Markov chain Monte Carlo (MCMC). Upon sufficiently sampling from $q\Big(\boldsymbol{x}\Big|I\big(F_i(\boldsymbol{x}) \geq \mathcal{F}\big) = 1\Big)$, we construct the importance density $f(\boldsymbol{x})$ using these samples. Finally, we sample from $f(\boldsymbol{x})$ and estimate the failure probability by using Equation (15). Figure 6 illustrates AIS, in which (1) an MCMC sampler always results in samples corresponding to failed TRISO particles, (2) these samples are used to construct the importance density $f(\boldsymbol{x})$, and (3) the constructed $f(\boldsymbol{x})$ is appropriate because it is nearly proportional to $[I\big(F_i(\boldsymbol{x}) \geq \mathcal{F}\big) = 1]\ q(\boldsymbol{x})$ and can sufficiently sample from the input parameter space resulting in numerous TRISO failures.

Following Au and Beck [1], for sampling from $q\Big(\boldsymbol{x}\Big|I\big(F_i(\boldsymbol{x}) \geq \mathcal{F}\big) = 1\Big)$ using MCMC, assume we have an input sample $\boldsymbol{x}^1$ that causes the TRISO model to fail. A proposal distribution $\zeta(\boldsymbol{x})$ is then selected, and a new sample $\boldsymbol{x}^*$ is proposed from this distribution. the MCMC sampling is performed by transforming all the input parameters $\boldsymbol{x}$ into a standard normal space, and by using a multivariate Gaussian with a covariance as an identity matrix centered around $\boldsymbol{x}^i$ as the proposal distribution $\zeta(\boldsymbol{x}|\boldsymbol{x}^i)$. Note that this choice of $\zeta(\boldsymbol{x})$ is a symmetric distribution permitting the use of the Metropolis algorithm without the correction proposed by Hastings for non-symmetric proposals. With $\zeta(\boldsymbol{x}|\boldsymbol{x}^i)$ being a symmetric distribution, the Metropolis acceptance ratio ($\alpha$) is computed to decide whether or not to accept $\boldsymbol{x}^*$:

$$\alpha^{i+1} = \frac{I\big(F_i(\boldsymbol{x}) \geq \mathcal{F}\big)\ \boldsymbol{\mathcal{N}}(\boldsymbol{x}^*)}{\boldsymbol{\mathcal{N}}(\boldsymbol{x}^i)} \qquad \big[\boldsymbol{\mathcal{N}}() \text{ is a standard multivariate Gaussian}\big] \tag{17}$$

which is accepted only if $\alpha_{i+1}$ is greater than a uniformly distributed random variable bounded by $[0,\ 1]$. The process of proposing $\boldsymbol{x}^*$ from $\zeta(\boldsymbol{x})$ and evaluating $\alpha_{i+1}$ in terms of whether or not to accept $\boldsymbol{x}^*$ is repeated until a sufficient number of importance samples is generated. According to Au and Beck [1], $\boldsymbol{x}^1$ may be deterministically selected using expert judgement, or probabilistically selected by running a few

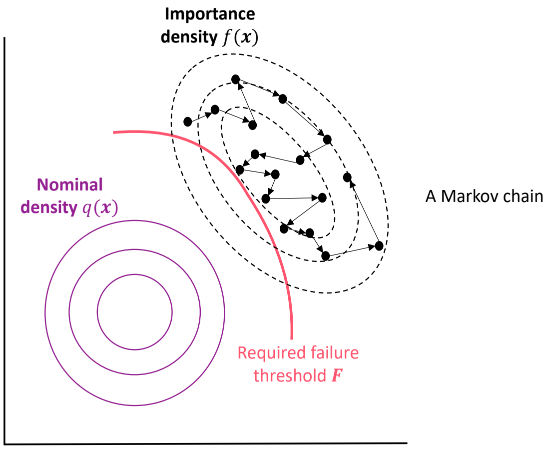


Figure 6: Adaptive importance sampling with a Markov chain characterizing the importance density that results in model failures.

TRISO evaluations. Additionally, $\boldsymbol{x}^i$ represents a previously accepted sample that causes the TRISO model to fail. Upon sufficiently sampling from $q\Big(\boldsymbol{x}\Big|I\big(F_i(\boldsymbol{x}) \geq \mathcal{F}\big) = 1\Big)$ using MCMC, we employed an uncorrelated multivariate Gaussian importance distribution—unlike Au and Beck [1], who used a multivariate kernel density to construct the importance distribution. In our assessments of several TRISO models, an uncorrelated multivariate Gaussian led to more robust failure probability estimation than when using a multivariate kernel density. Sampling from this importance density $f(\boldsymbol{x})$ was performed to evaluate Equation (15). If $M$ is the total number of TRISO evaluations, then $M = P + N$, with $P$ evaluations to sample from $q\Big(\boldsymbol{x}\Big|I\big(F_i(\boldsymbol{x}) \geq \mathcal{F}\big) = 1\Big)$ using MCMC, and $N$ evaluations to sample from $f(\boldsymbol{x})$ to estimate $\hat{P}_f^{\text{AIS}}$. The variance of $\hat{P}_f^{\text{AIS}}$ was estimated via [1]:

$$\text{Var}(\hat{P}_f^{\text{AIS}}) = \frac{1}{N}\left\{\frac{1}{N}\sum_{i=1}^{N}\left[I\big(F_i(\boldsymbol{x}) \geq \mathcal{F}\big)\ \frac{q(\boldsymbol{x})}{f(\boldsymbol{x})}\right]^2 - \big(\hat{P}_f^{\text{AIS}}\big)^2\right\} \tag{18}$$

and the COV was estimated via:

$$\hat{\delta}^{\text{AIS}} = \frac{\sqrt{\text{Var}(\hat{P}_f^{\text{AIS}})}}{\hat{P}_f^{\text{AIS}}} \tag{19}$$

As presented in Figure 6, a single Markov chain in this version of AIS was used to construct the importance density. Since samples from MCMC are history dependent, it is impossible to parallelize AIS by simultaneously conducting the TRISO evaluations on several different processors. Therefore, in general, the computational efficiency of AIS when run using a single processor on a local machine would be similar to that of either MCS or LHS run using hundreds of processors on a supercomputer. The SS method, discussed next, uses numerous independent Markov chains and is thus parallelizable.

### *3.4. Variance reduction method: subset simulation*

SS is another popular variance reduction method for estimating small failure probabilities [2]. Unlike AIS, it can be parallelized, as it relies on numerous independent Markov chains to estimate failure probabilities, and does not require specification of a starting input value ($\boldsymbol{x}^1$) that causes the TRISO model to fail. The basic idea of SS is to express a small failure probability as the product of $N_s$ larger failure probabilities, such that the total probability theorem is satisfied [2]:

$$\hat{P}_f^{\text{SS}} = \hat{P}_1^{\text{SS}} \prod_{i=2}^{N_s} \hat{P}_{i|i-1}^{\text{SS}} \tag{20}$$

where $\hat{P}_1^{\text{SS}} = \hat{P}_1^{\text{SS}}\big(F(\boldsymbol{x}) > \mathcal{F}_1\big)$ is the first unconditional failure probability and $\hat{P}_{i|i-1}^{\text{SS}} = \hat{P}_{i|i-1}^{\text{SS}}\big(F(\boldsymbol{x}) > \mathcal{F}_i \mid F(\boldsymbol{x}) > \mathcal{F}_{i-1}\big)$ is the $i^{th}$ $\big(i \in [2, 3, \dots, N_s]\big)$ conditional failure probability. Using intermediate failure probabilities ($\hat{P}_1^{\text{SS}}$ and $\hat{P}_{i|i-1}^{\text{SS}}$) creates intermediate failure thresholds $\big(\text{i.e., } \mathcal{F}_i\ (i \in [1, 2, \dots, N_s - 1])\big)$ before the required failure threshold. The region of the input parameter space bounded between two successive intermediate failure thresholds is termed the subset. Also, $\mathcal{F}_{N_s} = \mathcal{F}$ is the required failure threshold. Figure 7 illustrates these intermediate failure thresholds. Either the intermediate failure thresholds can be specified a priori, in which case $\hat{P}_1^{\text{SS}}$ and $\hat{P}_{i|i-1}^{\text{SS}}$ in Equation (20) must be estimated, or $\hat{P}_1^{\text{SS}}$ and $\hat{P}_{i|i-1}^{\text{SS}}$ can be specified a priori, in which case the intermediate failure thresholds should be computed. The latter approach is more popular, with $\hat{P}_1^{\text{SS}}$ and $\hat{P}_{i|i-1}^{\text{SS}}$ $(i \in [2, 3, \dots, N_{s-1}])$ all usually being set to 0.1, and $\hat{P}_{N_s|N_{s-1}}^{\text{SS}}$ being estimated by counting the fraction of samples that exceed the required failure threshold $\mathcal{F}$. Since $\hat{P}_{N_s|N_{s-1}}^{\text{SS}}$ is a conditional failure probability, generating conditional samples for estimating it requires determination of the intermediate failure threshold $\mathcal{F}_{N_{s-1}}$. In turn, determination of $\mathcal{F}_{N_{s-1}}$ depends on the determinations of all the previous intermediate failure thresholds $\mathcal{F}_{N_{s-2}}, \dots, \mathcal{F}_2,\ \mathcal{F}_1$.

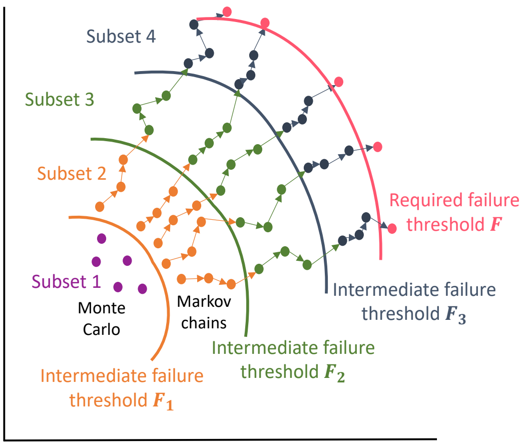


Figure 7: SS with numerous Markov chains exploring the input parameter space to efficiently reach the required failure threshold at some point.

In practice, SS is implemented in the following manner. If $N$ is the total number of TRISO evaluations, each subset will have $M = N/N_s$ samples. An MCS is first used to generate $M$ samples, as represented by the purple dots in Figure 7. If the intermediate failure probabilities (except $\hat{P}_{N_s|N_{s-1}}^{\text{SS}}$) are all fixed to 0.1, then the first intermediate failure threshold $\mathcal{F}_1$ is estimated as the 90$^{\text{th}}$ percentile value of all the $M$ sample outputs. The samples' outputs that do not exceed $\mathcal{F}_1$ constitute Subset 1. To determine the next failure threshold $\mathcal{F}_2$, conditional samples should be generated such that the TRISO model outputs always exceed $\mathcal{F}_1$. An MCMC method—in particular, a component-wise Metropolis method—is used to estimate $\mathcal{F}_2$ by simulating several Markov chains, as presented in Figure 7. From the $M$ MCS samples, those that exceeded the threshold $\mathcal{F}_1$ are used as seeds (or starting values) for the Markov chains. If $M$ samples need to be simulated such that the outputs exceed $\mathcal{F}_1$, there will be $\texttt{int}(0.1\ M)$ Markov chains, with each chain simulating $\texttt{int}(1/0.1)$ samples (where $\texttt{int}$ is the nearest integer operation). In general, if the intermediate failure probabilities in Equation (20) (except $\hat{P}_{N_s|N_{s-1}}^{\text{SS}}$) are fixed to $p_o$ instead of 0.1, there will be $\texttt{int}(p_o\ M)$ Markov chains, with each chain simulating $\texttt{int}(1/p_o)$ samples. For simulating a Markov chain, the components $x_j$ are all first transformed into a standard normal space, and a Gaussian whose unit variance is centered around $x_j^k \in \boldsymbol{x}^k$ is used as the proposal distribution $\zeta(x_j)$. A new sample $x_j^*$ is proposed from the symmetric proposal distribution $\zeta(x_j)$ for the $j^{\text{th}}$ input parameter in the vector $\boldsymbol{x}$ (i.e., $x_j \in \boldsymbol{x}$). The Metropolis acceptance ratio is computed as:

$$\alpha^{k+1} = \frac{\mathcal{N}(x_j^*)}{\mathcal{N}(x_j^k)} \qquad \big[\mathcal{N}() \text{ is a standard Gaussian}\big] \tag{21}$$

where the proposed sample $x_j^*$ is only accepted if $\alpha_{k+1}$ is greater than a uniformly distributed random variable bounded by [0, 1]. The Metropolis acceptance step is repeated for all the parameters in the vector $\boldsymbol{x}$. Accepted components represent the vector $\boldsymbol{x}^*$, which is only accepted as the new sample $\boldsymbol{x}^{k+1}$ if the TRISO output exceeds the threshold $\mathcal{F}_1$. $\boldsymbol{x}^k$ is a previously accepted sample whose TRISO output has exceeded the failure threshold $\mathcal{F}_1$. If $k = 1$, $\boldsymbol{x}^1$ is the seed sample for the Markov chain. Once $M$ samples are generated from $\texttt{int}(p_o\ M)$ Markov chains, the second intermediate failure threshold $\mathcal{F}_2$ is the $(1-p_o)\times 100$ percentile value of all the samples' outputs. Samples between $\mathcal{F}_1$ and $\mathcal{F}_2$ comprise the second subset, as presented in Figure 7. A similar procedure of simulating $\texttt{int}(p_o\ M)$ Markov chains is repeated for determining the subsequent failure thresholds until the final required failure threshold $\mathcal{F}$ is reached. More details on the practical implementation of the SS method are presented in Li and Cao [13].

Since there are multiple intermediate failure probabilities in SS, each has an associated COV value. The COV for the $i^{\text{th}}$ subset is estimated as:

$$\hat{\delta}_i^{\text{SS}} = \sqrt{\frac{1-P_i}{P_i\ M}} \quad \text{where, } P_i = \begin{cases} P_1\ \forall\ i = 1 \\ \hat{P}^{\text{SS}}_{i|i-1}\ \forall\ i \in [2,\ldots,N_s] \end{cases} \tag{22}$$

The COV of the failure probability estimate of Equation (20) is computed as:

$$\hat{\delta}^{\text{SS}} = \sqrt{\sum_{i=1}^{N_s} \left(\hat{\delta}_i^{\text{SS}}\right)^2} \tag{23}$$

Equation (23) is an approximation to the COV, as it ignores the auto-correlations between samples in a Markov chain. Au and Beck [2] proposed a more accurate COV estimate that considers such auto-correlations. Furthermore, Shields et al. [27] refined the COV estimate proposed by Au and Beck [2] to also consider the cross correlations between different Markov chains. In practice, it is still common to estimate the COV using Equation (23) [13] although it underestimates the COV.

Since the SS method consists of numerous Markov chains in each subset, the TRISO evaluations for separate Markov chains can be conducted in parallel using multiple processors. It is important to note that parallelization is only feasible across Markov chains, and not within a given chain. A single processor should be used to completely evaluate an entire Markov chain consisting of $\texttt{int}(1/p_o)$ samples. Also, subset $i+1$ cannot begin before simulating subset $i$ which means that a single processor should at least evaluate $\texttt{int}(1/p_o)\ N_s$ samples. If there are $P$ processors and $\texttt{int}(p_o\ M)\ N_s$ samples across all the subsets, each processor evaluates the following number of samples:

$$N_P^{\text{SS}} = \max \begin{cases} \frac{\texttt{int}(p_o\ M)\ N_s}{P} \\ \texttt{int}(1/p_o)\ N_s \end{cases} \tag{24}$$

where $N_P^{\text{SS}}$ is the number of samples per processor in the parallel SS implementation. Figures 8a and 8b present the samples-per-processor comparison between SS and MCS for COV values of 0.1 and 0.05, respectively, considering the failure probabilities $1E-4$ and $1E-6$. In general, the parallel SS method requires significantly fewer TRISO evaluations per processor than MCS, especially for lower failure probabilities and/or a low COV. Owing to this computational efficiency of parallel SS, it is possible to directly evaluate the 2-D TRISO model without making the 1-D approximation, as discussed in Section 5. Notice that, in both Jiang et al. [12] and PARFUME [19], TRISO failure evaluations relied on an approximate 1-D model because it is computationally infeasible to use the 2-D model in a MCS method, even with parallel computing.

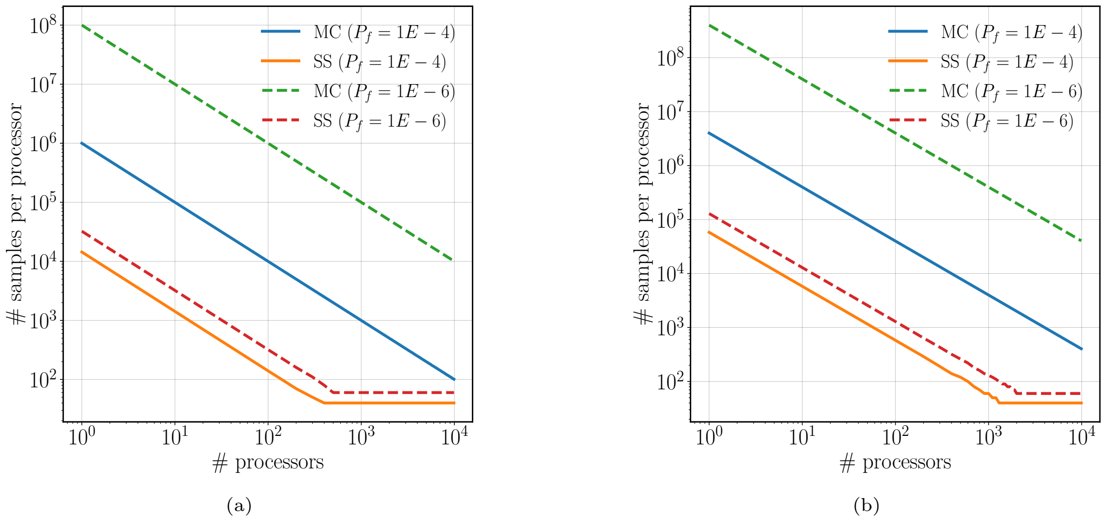


Figure 8: Comparison of samples per processor between MCS and SS, considering the two failure probabilities of $1E-4$ and $1E-6$, and COVs of (a) 0.1 and (b) 0.05. For SS, these plots assume that each processor runs one complete Markov chain per subset consisting of $1/p_o$ samples.

### *3.5. Distribution sampling: the Weibull theory*

As explained in Section 2.3, a Weibull criterion is used to determine failure of the IPyC and SiC layers. This means that, for a given set of random input parameters and the computed stresses in the IPyC and SiC layers, we can estimate the Weibull failure probability using the CDF of a Weibull distribution:

$$W_i(\boldsymbol{x}) \sim 1 - \exp\Bigg( - \frac{\sigma_c(\boldsymbol{x})^m}{(\sigma_{ms})^m}\Bigg) \tag{25}$$

where $\sigma_c(\boldsymbol{x}$ is the stress in either the IPyC or SiC layers, $\sigma_{ms})$ is the mean strength of either IPyC or SiC, $m$ is the Weibull modulus of either IPyC or SiC, and $W_i(\boldsymbol{x})$ is a realization of the Weibull failure probability. $W_i(\boldsymbol{x})$ will be random due to the randomness in the input parameters. Therefore, the mean failure probability of either the IPyC or SiC layer cracking is given by replacing the indicator function in Equation (8) with the realization of the Weibull failure probability for sample $i$:

$$\hat{P}_f^{\mathrm{W}} = \frac{1}{N} \sum_{i=1}^{N} W_i(\boldsymbol{x}) \tag{26}$$

The COV over the failure probability estimate is given as:

$$\hat{\delta}^{\mathrm{W}} = \frac{1}{\hat{P}_f^{\mathrm{W}}} \sqrt{\frac{\sum_{i=1}^{N} W_i(\boldsymbol{x})^2}{N^2} - \frac{(\hat{P}_f^{\mathrm{W}})^2}{N}} \tag{27}$$

Note that, in Equations (26) and (27), unlike when using the other Monte Carlo approaches, the strengths of the IPyC and SiC layers are not part of the input parameter vector $\boldsymbol{x}$. As the failure probability is estimated by averaging the Weibull failure probabilities, the COV is expected to decrease rapidly as the number of samples increases. Figure 9 illustrates that the COV is less than a mere 0.05 for 100 evaluations of the TRISO model. It is therefore possible to directly use the 2-D TRISO model to estimate the failure probability via the Weibull theory.

Although the Weibull theory is computationally inexpensive for estimating failure probabilities, it does not directly provide information on the distributions of input parameters that cause IPyC and/or SiC failures. Such information can be crucial for optimizing fuel design and fabrication [7]. Also, TRISO fuel can have other failure modes (e.g., kernel migration [19]) not characterized by the Weibull failure criterion.

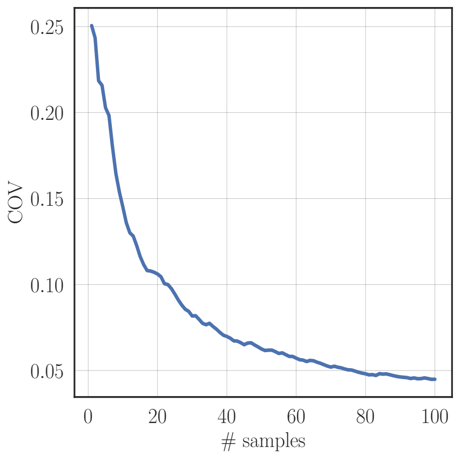


Figure 9: COV evolution with number of samples when using the Weibull theory.

The Weibull theory cannot accommodate these additional failure criteria, unlike the other Monte Carlo approaches presented previously.

## 4. Statistical failure analysis considering 1-D TRISO models

In this section, the failure probabilities and distributions of input parameters that cause TRISO failure are compared across the four Monte-Carlo-based approaches and the Weibull theory discussed earlier. One-dimensional versions of the four TRISO models discussed in Section 2.4 are considered. It is noted that, in the 1-D TRISO model, IPyC layer cracking is not directly simulated, and the effects of cracking (e.g., stress concentration in the SiC layer) are accounted for by stress modification factors. In addition, the 1-D TRISO model assumes spherical symmetry, meaning that the effects of particle asphericity (itself a result of the fuel fabrication process) on SiC layer stresses must also be accounted for through stress modification factors. These modification factors were discussed in Section 2.3. Finally, the TRISO model is considered to have failed if the SiC stresses exceed its strength, either due to IPyC cracking or particle asphericity. Such failure criterion details were also discussed in Section 2.3.

### *4.1. Failure probability estimates*

Table 4 provides the failure probabilities ($\hat{P}_f$), COV values ($\hat{\delta}$), and number of TRISO model evaluations ($N$) for the four models and five Monte-Carlo-based methods. These $\hat{P}_f$ values account for the three failure modes (i.e., SiC failure due to IPyC cracking and pressure vessel failure for spherical and aspherical particles) as discussed in Section 2.3. However, it was found across the four models that SiC failure due to IPyC cracking is the most dominant failure mode and has $\hat{P}_f$ values that are at least 3-4 orders of magnitude greater than the other two failure modes. The MCS, LHS, and SS methods were run using parallel computing on 1,000 processors. The number of TRISO evaluations per processor when using these methods was $N/1000$. For each of the five methods, we performed enough TRISO evaluations to ensure that the COV values were mostly between $\sim 0.05$ and $\sim 0.1$, providing a similar basis for comparisons between the methods. For the AIS method, it is infeasible to determine a priori the number of required TRISO evaluations for a target COV value; and so for Model 4, the COV value is 0.15, even with $1E4$ evaluations. There is good agreement among the $\hat{P}_f$ values obtained via the five methods across all four models taking into account the COV values. In addition, these $\hat{P}_f$ values are in agreement with the study by Jiang et al. [12] which verified Bison results with the PARFUME code [19]. For model 3, the failure probabilities seem higher because this case corresponds to the benchmark verification case with PARFUME from Jiang et al. [12]. Variance reduction methods such as AIS and SS, which aim to reduce the number of evaluations of the

TRISO model, may be preferred over MCS and LHS, which require a large number of model evaluations. With the use of parallel computing, MCS and LHS require a total wall clock time (or, elapsed time since the simulation begins) similar to AIS, which can only be run in a serial fashion. Parallel SS requires a much smaller number of TRISO evaluations per processor than either AIS or parallel MCS and LHS. Even with serial computing, the number of TRISO evaluations per processor required by the Weibull theory is similar to that required by parallel SS. However, the Weibull theory does not provide additional information such as the statistics of failure-causing input parameters.

Table 4: Failure probabilities, COVs, and number of 1-D TRISO evaluations for five different statistical methods across four models.

| | **QoI** | **Monte Carlo Sampling (MCS)** | **Latin Hypercube Sampling (LHS)** | **Adaptive Importance Sampling (AIS)**[†] | **Subset Simulation (SS)** | **Weibull approach (W)** |
|---|---|---|---|---|---|---|
| Model 1 (Spherical) | $\hat{P}_f$ | $1.05E-4$ | $1.05E-4$ | $1E-4$ | $1.27E-4$ | $1.01E-4$ |
| | $\hat{\delta}$ | 0.098 | 0.098 | 0.073 | 0.056 | 0.042 |
| | $N$ | $1E6$ | $1E6$ | $1E4$ | $4E4$ | 100 |
| | $T$[‡] | 3.06 hrs | 3.06 hrs | — | 0.12 hrs | 0.31 hrs |
| | $P$ | 1000 | 1000 | 1 | 1000 | 1 |
| Model 2 (Spherical) | $\hat{P}_f$ | $3.84E-5$ | $3.2E-5$ | $3.29E-5$ | $4.52E-5$ | $3.29E-5$ |
| | $\hat{\delta}$ | 0.102 | 0.111 | 0.042 | 0.059 | 0.041 |
| | $N$ | $2.5E6$ | $2.5E6$ | $1E4$ | $4E4$ | 100 |
| | $T$[‡] | 7.64 hrs | 7.64 hrs | — | 0.12 hrs | 0.31 hrs |
| | $P$ | 1000 | 1000 | 1 | 1000 | 1 |
| Model 3 (Aspherical) | $\hat{P}_f$ | $9.26E-4$ | $8.6E-4$ | $7.69E-4$ | $8.92E-4$ | $8.33E-4$ |
| | $\hat{\delta}$ | 0.085 | 0.088 | 0.073 | 0.052 | 0.045 |
| | $N$ | $1.5E5$ | $1.5E5$ | $1E4$ | $4E4$ | 100 |
| | $T$[‡] | 0.46 hrs | 0.46 hrs | — | 0.12 hrs | 0.31 hrs |
| | $P$ | 1000 | 1000 | 1 | 1000 | 1 |
| Model 4 (Aspherical) | $\hat{P}_f$ | $1.45E-5$ | $1.31E-5$ | $1.6E-5$ | $1.87E-5$ | $1.39E-5$ |
| | $\hat{\delta}$ | 0.083 | 0.087 | 0.15 | 0.063 | 0.061 |
| | $N$ | $1E7$ | $1E7$ | $1E4$ | $4E4$ | 100 |
| | $T$[‡] | 30.6 hrs | 30.6 hrs | — | 0.12 hrs | 0.31 hrs |
| | $P$ | 1000 | 1000 | 1 | 1000 | 1 |

**Abbreviation** QoI: Quantity of Interest
**Notations** $\hat{P}_f$: Failure probability estimate; $\hat{\delta}$: COV estimate; $N$: number of TRISO evaluations across all the processors; $T$: Average elapsed time; $P$: Number of processors used
[‡] Computed by multiplying the average time for each model evaluation (i.e., 11 seconds) with the number of evaluations per processor
[†] AIS samples mostly from the model failure region and each model evaluation takes less time than the average time. These simulation times were not recorded and hence not reported in this table.

### *4.2. Distributions of input parameters that cause TRISO failures*

Figure 10 presents, for Model 1, the empirical CDF (eCDF) plots of the distributions of input parameters that cause TRISO failures. Along with the eCDF plots from the four Monte-Carlo-based methods, the nominal (or given) distributions of the input parameters are also provided. Note that all the distributions are transformed into a standard normal space using a one-to-one mapping, thus establishing a common basis for making comparisons across the input parameters. The IPyC and SiC strengths are the most sensitive input parameters, as seen from Figure 10, and all four methods quite consistently represent these sensitivities, manifested by similar eCDF plots. While the eCDF plots for the four methods are quite consistent for most of the input parameters, the kernel radius eCDF for the AIS method is quite different from that obtained with the other methods. The AIS method uses a single Markov chain to explore the input parameter space, as discussed in Section 3.3. Such a localized random walk may lead to underexploration of the input space and mischaracterization of the failure-causing-parameter distributions, especially when the TRISO failure is not sensitive to the parameter of interest. From both Jiang et al. [12] and Skerjanc et al. [28], TRISO failures are known to be negligibly sensitive to the kernel radius. The parallel SS method improves on the AIS method, as it uses hundreds of Markov chains (as opposed to just one) to better explore the input space (see Section 3.4). As parallel SS is a computationally effective approach for characterizing TRISO failure, its performance compared with MCS (which is generally considered reliable) is studied next in more detail.

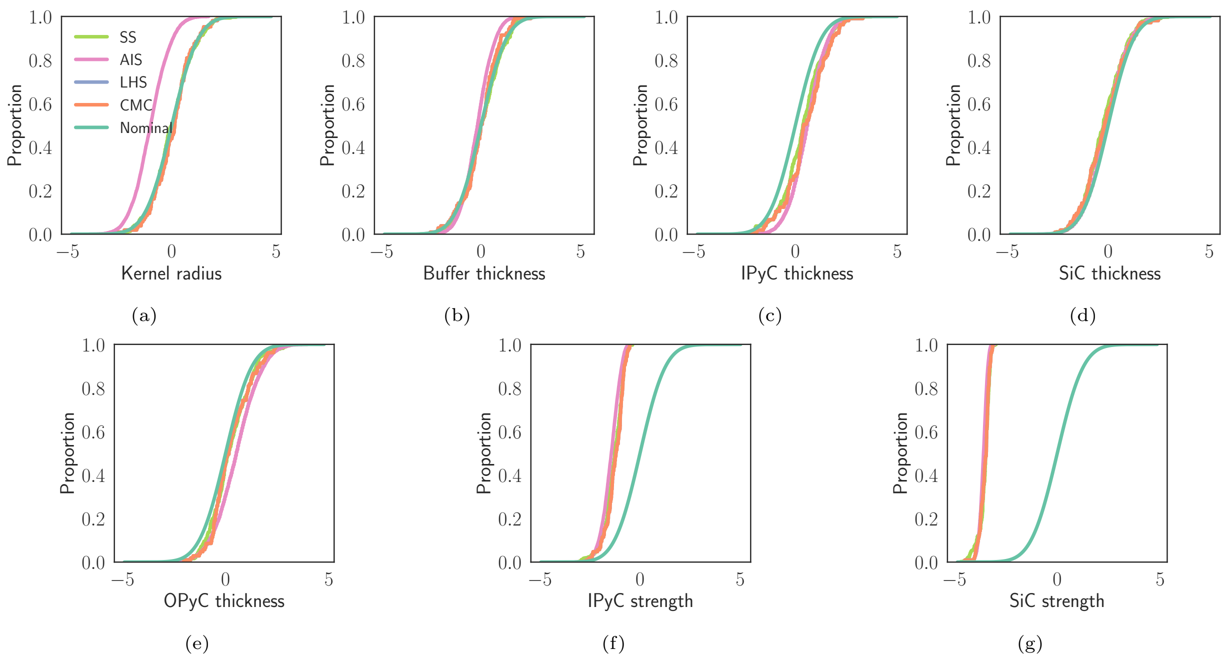


Figure 10: Empirical cumulative distribution functions of failure-causing input parameters for the five statistical methods applied to TRISO Model 1 (1-D). The input parameters are (a) kernel radius, (b) buffer thickness, (c) IPyC thickness, (d) SiC thickness, (e) OPyC thickness, (f) IPyC strength, and (g) SiC strength. All distributions are transformed into a standard normal space.

For TRISO Model 1, Figure 11 presents a grid plot of the TRISO-failure-causing input parameter distributions and correlations for both the MCS and SS methods. While the plot diagonals compare the kernel density distributions of MCS and SS, the off-diagonals compare the correlations of the parameters in terms of scatter plots (lower off-diagonal) and kernel contour plots (upper off-diagonal). It is again noted that all distributions were transformed into a standard normal space using a one-to-one mapping. Overall, good agreement between the MCS and SS methods is found in both the individual parameter distributions (the diagonals in Figure 11) and their correlations (the off-diagonals in Figure 11).

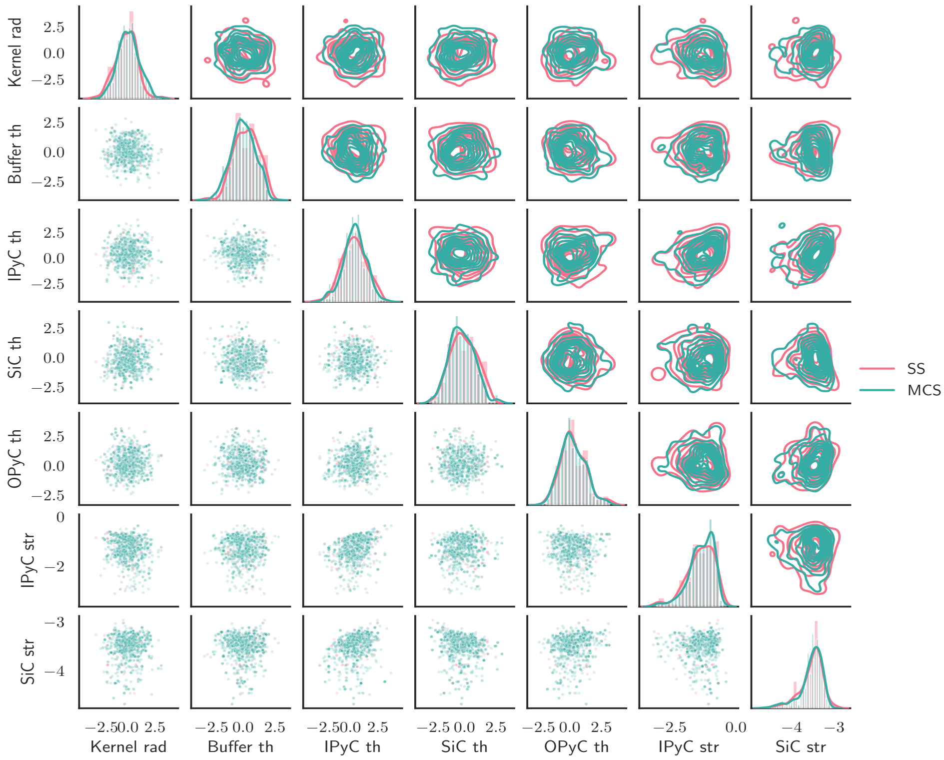


Figure 11: Pair grid plot of failure-causing input parameter distributions for TRISO Model 1 (1-D), using the MCS and SS methods. The diagonals represent kernel densities, and the upper and lower diagonals represent kernel contour plots and scatter plots of input parameter pairs, respectively. All distributions are transformed into a standard normal space. (**Abbreviations** rad: radius; th: thickness; and str: strength)

Figure 12 presents the mean values of the failure-causing input parameters under the MCS and SS methods for all four considered models. Also presented in Figure 12 are the nominal mean values of these parameters, which are all zeroes due to the transformation into a standard normal space. Overall, the MCS and SS methods show good agreement in the mean failure-causing-parameter values across the four models. The strengths of SiC and IPyC are the most sensitive parameters to TRISO failures, with lower strength values causing more failures. IPyC thickness is second in terms of TRISO failure sensitivity, with higher thickness values causing more failures. Also, lesser SiC thicknesses are seen to cause more TRISO failures. The other input parameters are seen to be less sensitive to TRISO failures. These observations mostly align with the conclusions drawn by Jiang et al. [12] and Skerjanc et al. [28] regarding the effects of input parameters on TRISO failures. Also, for model 3, the mean value of the failure-causing IPyC strength is not very different from the nominal case. This is due to the comparatively lower temperature of model 3 than the other models as discussed in Section 2.4 which is not causing enough creep and stress relaxation in the IPyC layer. Therefore, the stresses in the IPyC layer, in general, are higher than the other three models causing more IPyC failures and showing no significant difference in the mean IPyC strength between the failure-causing and nominal cases.

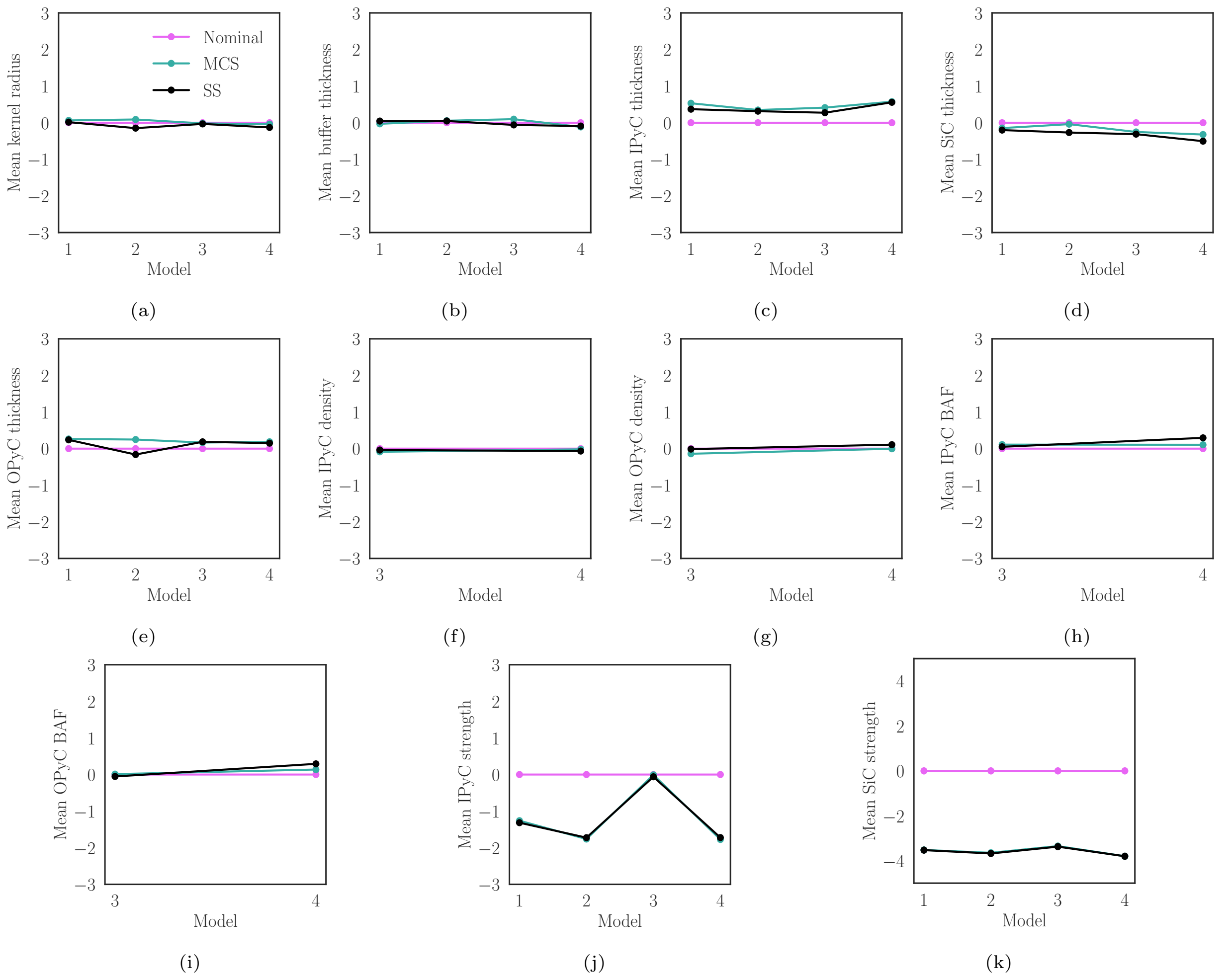


Figure 12: Mean values of the failure-causing input parameters, as computed by applying the MCS and SS methods on all four 1-D TRISO models. All distributions are transformed into a standard normal space. Note that some parameters are not shown for Models 1 and 2 because they were held constant.

## 5. Statistical failure analysis considering 2-D TRISO models

Because of the large number of evaluations required by the commonly-used statistical analysis methods and the relatively high computational cost of 2-D models, statistical analyis of TRISO fuel has generally been limited to using 1-D models in conjunction with techniques such as the stress modification factors described in Section 2.3 to capture higher-dimensional effects. The SS method and Weibull theory have a demonstrated ability to provide accurate failure probability estimates with a small number of samples, so it is reasonable to expect that these approaches could be directly applied to 2-D models for improved accuracy with a relatively modest computational cost. Moreover, due to its higher fidelity, the 2-D model results can be more accurate than the 1-D model. In this section, 2-D versions of the four TRISO models discussed in Section 2.4 are considered using the parallel SS method and Weibull theory, and the results of these simulations are assessed.

### *5.1. Modeling details*

The 2-D model is an axisymmetric model of the TRISO particle. Instead of using line elements to represent each of the TRISO layers, the 2-D model is composed of rings. Cracking in the IPyC layer can be directly modeled using the XFEM mesh-cutting module [11] within Bison. Particle asphericity can also be directly accounted for in the 2-D model. Neither of these phenomena, which are a departure from spherical symmetry, can be represented directly in a 1-D model. Figures 13a and 13b present the finite element mesh of a spherical and aspherical 2-D model, respectively. In these models, the kernel, buffer, IPyC, SiC, and OPyC layers have 20, 8, 5, 3, and 4 elements in the radial direction, respectively. These layers have 60 elements in the circumferential direction. Both the IPyC and SiC layers are considered failed if the stress exceeds their strength. Since the SiC layer can fail mostly fails due to IPyC cracking, its failure is modeled in two stages: (1) fracture initiation in the IPyC layer, with no explicit representation of a crack; and (2) SiC failure that is conditional on IPyC failure, with XFEM being used to represent a crack in the IPyC layer at the start of the simulation. Particle asphericity, if present, is considered automatically in a 2D TRISO model through the mesh geometry. The probability of SiC layer failure is computed as follows:

$$P(\text{SiC fail}) = P(\text{SiC fail} \mid \text{IPyC fail})\ P(\text{IPyC fail}) + P(\text{SiC fail due to pressure vessel}) \tag{28}$$

$P(\text{SiC fail} \mid \text{IPyC fail})$ and $P(\text{IPyC fail})$ are computed independently, then multiplied to calculate the final failure probability of the SiC layer due to IPyC cracking. We did not explicitly calculate $P(\text{SiC fail due to pressure vessel})$ in view of the computational expense because it is at least 3-4 orders of magnitude smaller than SiC layer failure due to IPyC cracking, as noted in the 1D TRISO model discussion in Section 4.1, even in the presence of asphericity and its contribution to the overall SiC failure would be negligible.

(a) (b)

Figure 13: 2-D axisymmetric mesh of a TRISO particle with (a) no asphericity and (b) asphericity. (Gray: kernel; red: buffer; green: IPyC; blue: SiC; and yellow: OPyC)

### *5.2. Failure probability estimates*

The failure probability of the TRISO particles is computed by applying the SS and Weibull methods to the 2-D TRISO model. The other Monte-Carlo-type methods discussed in Section 3 are computationally prohibitive for use with the 2-D TRISO model, and the AIS algorithm cannot be used in parallel, which similarly limits its applicability to the 2-D TRISO model. For the SS method, $4E4$ and $1E4$ evaluations were used to independently compute $P(\text{SiC fail} \mid \text{IPyC fail})$ and $P(\text{IPyC fail})$ in Equation (28), respectively. The SS method was used with 1,000 processors, each of which evaluated the 2-D TRISO model 40 and 10 times for $P(\text{SiC fail} \mid \text{IPyC fail})$ and $P(\text{IPyC fail})$, respectively. For the Weibull method, $P(\text{SiC fail} \mid \text{IPyC fail})$ and $P(\text{IPyC fail})$ were each computed using 100 2-D TRISO evaluations. Table 5 presents the results for the four 2-D models. For comparison, the 1-D TRISO model results are also presented. All failure probabilities in Table 5 have a similar COV of around 0.05. In terms of 2-D modeling, both the SS and Weibull methods generate similar failure probability estimates across all four models. Also, in general, the 1-D and 2-D failure probability estimates show good agreement. The 1-D and 2-D results compare better for model 1 and 2 which are the spherical particle cases than for models 3 and 4 which are the aspherical particle cases, where higher failure probabilities are predicted for the 2-D model than for the 1-D model. In addition, as noted from Section 2.4, models 3 and 4 have lower temperatures than models 1 and 2. The results from the 2-D model can be sensitive to mesh density, especially at lower temperatures and under particle asphericity. For example, in regard to Model 4, when the mesh was made twice as dense as the one presented in Figure 13b, the failure probability estimate generated via the Weibull method was $2.56E-5$, agreeing slightly better with the 1-D model. However, the computational expense for a single sample increased from $\sim 0.55$ hours using the mesh in Figure 13b to $\sim 9$ hours using the denser mesh. Additionally, the quality of the approximation made by the 1-D model's stress modification factors in Section 2.4 is also responsible to the differences in the 1-D and 2-D results. In conclusion, the mesh density and approximation quality of the 1-D model's stress modification factors can explain the differences between the 2-D and 1-D model results under lower temperatures and particle asphericity.

Table 5: Failure probabilities, COVs, and number of 2-D TRISO evaluations for the SS and Weibull methods across four models. The corresponding 1-D model results are also presented for comparison.

| | **QoI** | **Subset Simulation** | **Weibull approach** | **Subset Simulation** | **Weibull approach** |
|---|---|---|---|---|---|
| | | **2-D TRISO model** | | **1-D TRISO model** | |
| Model 1 (Spherical) | $\hat{P}_f$ | $1.19E-4$ | $0.99E-4$ | $1.27E-4$ | $1.01E-4$ |
| | $\hat{\delta}$ | 0.055 | 0.04 | 0.056 | 0.042 |
| | $N$ | $5E4$ | 200 | $4E4$ | 100 |
| | $T^{\ddagger}$ | 27.5 hrs | 27.5 hrs | 0.12 hrs | 0.31 hrs |
| | $P$ | 1000 | 4 | 1000 | 1 |
| Model 2 (Spherical) | $\hat{P}_f$ | $3.4E-5$ | $5.86E-5$ | $4.52E-5$ | $3.29E-5$ |
| | $\hat{\delta}$ | 0.06 | 0.041 | 0.059 | 0.041 |
| | $N$ | $5E4$ | 200 | $4E4$ | 100 |
| | $T^{\ddagger}$ | 27.5 hrs | 27.5 hrs | 0.12 hrs | 0.31 hrs |
| | $P$ | 1000 | 4 | 1000 | 1 |
| Model 3 (Aspherical) | $\hat{P}_f$ | $2.49E-3$ | $2.42E-3$ | $0.89E-3$ | $0.83E-3$ |
| | $\hat{\delta}$ | 0.045 | 0.052 | 0.052 | 0.045 |
| | $N$ | $4E4$ | 200 | $4E4$ | 100 |
| | $T^{\ddagger}$ | 22 hrs | 27.5 hrs | 0.12 hrs | 0.31 hrs |
| | $P$ | 1000 | 4 | 1000 | 1 |
| Model 4 (Aspherical) | $\hat{P}_f$ | $3.75E-5$ | $3.84E-5$ | $1.87E-5$ | $1.39E-5$ |
| | $\hat{\delta}$ | 0.067 | 0.055 | 0.063 | 0.061 |
| | $N$ | $5E4$ | 200 | $4E4$ | 100 |
| | $T^{\ddagger}$ | 27.5 hrs | 27.5 hrs | 0.12 hrs | 0.31 hrs |
| | $P$ | 1000 | 4 | 1000 | 1 |

**Abbreviation** QoI: Quantity of Interest
**Notations** $\hat{P}_f$: Failure probability estimate; $\hat{\delta}$: COV estimate; $N$: number of TRISO evaluations across all the processors; $P$: Number of processors used
† Parallel computing was used
‡ Computed by multiplying the average time for each model evaluation (i.e., 33 minutes) with the number of evaluations per processor

*5.3. Input parameters that cause TRISO failures*

Considering Model 1, Figure 14 presents the pair grid plots of failure-causing input parameter distributions and densities for the SiC conditional on IPyC failures from the 2-D model simulations using the SS method. Also presented for comparison are the pair grid plots from the 1-D model SS results. An explanation of these pair grid plots was provided in Section 4.2. Overall, there is good agreement between the 2-D and 1-D model results in both the individual parameter distributions (the diagonals in Figure 14) and their correlations (the off-diagonals in Figure 14). Next, the mean values of the failure-causing input parameters for all four models are studied.

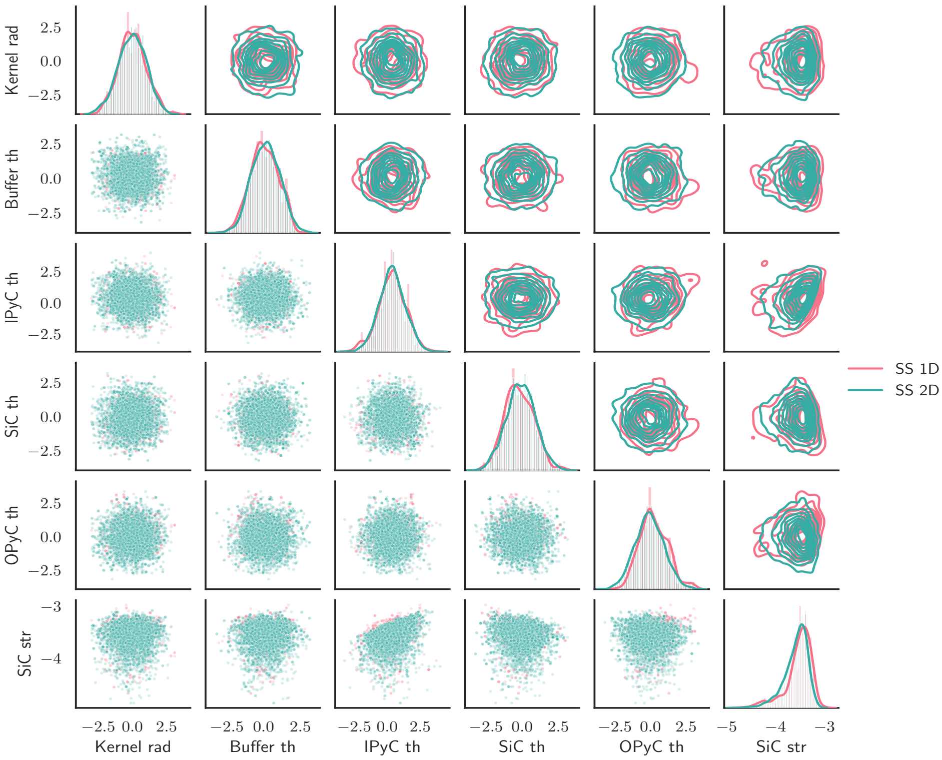


Figure 14: Pair grid plots of the SiC failure conditional on IPyC distributions of failure-causing input parameters for TRISO Model 1, in light of SS for 1-D and 2-D models. The diagonals represent kernel densities, and the upper and lower diagonals represent kernel contour plots and scatter plots of input parameter pairs, respectively. All distributions are transformed into a standard normal space. (**Abbreviations** rad: radius; th: thickness; and str: strength)

Figure 15 presents the mean values of the failure-causing input parameters computed via SS for all four 2-D and 1-D versions of the models. Overall, the 2-D and 1-D models show good agreement in the mean failure-causing parameter values across the four models. SiC layer strength is the parameter most sensitive to TRISO failure. Next, larger IPyC thicknesses are seen to cause more failures in both the 2-D and 1-D TRISO models. Also, while lesser SiC thicknesses are seen to cause more TRISO failures, the effect of SiC thickness is seen to be more pronounced in the 1-D models (especially models 3 and 4). Owing to asphericity, the results of the 2-D versions of models 3 and 4 are sensitive to mesh density. This sensitivity, coupled with the approximation quality of the stress modification factors for 1-D models, can explain the deviations in mean SiC thicknesses when comparing the 2-D and 1-D models (see Figure 15).

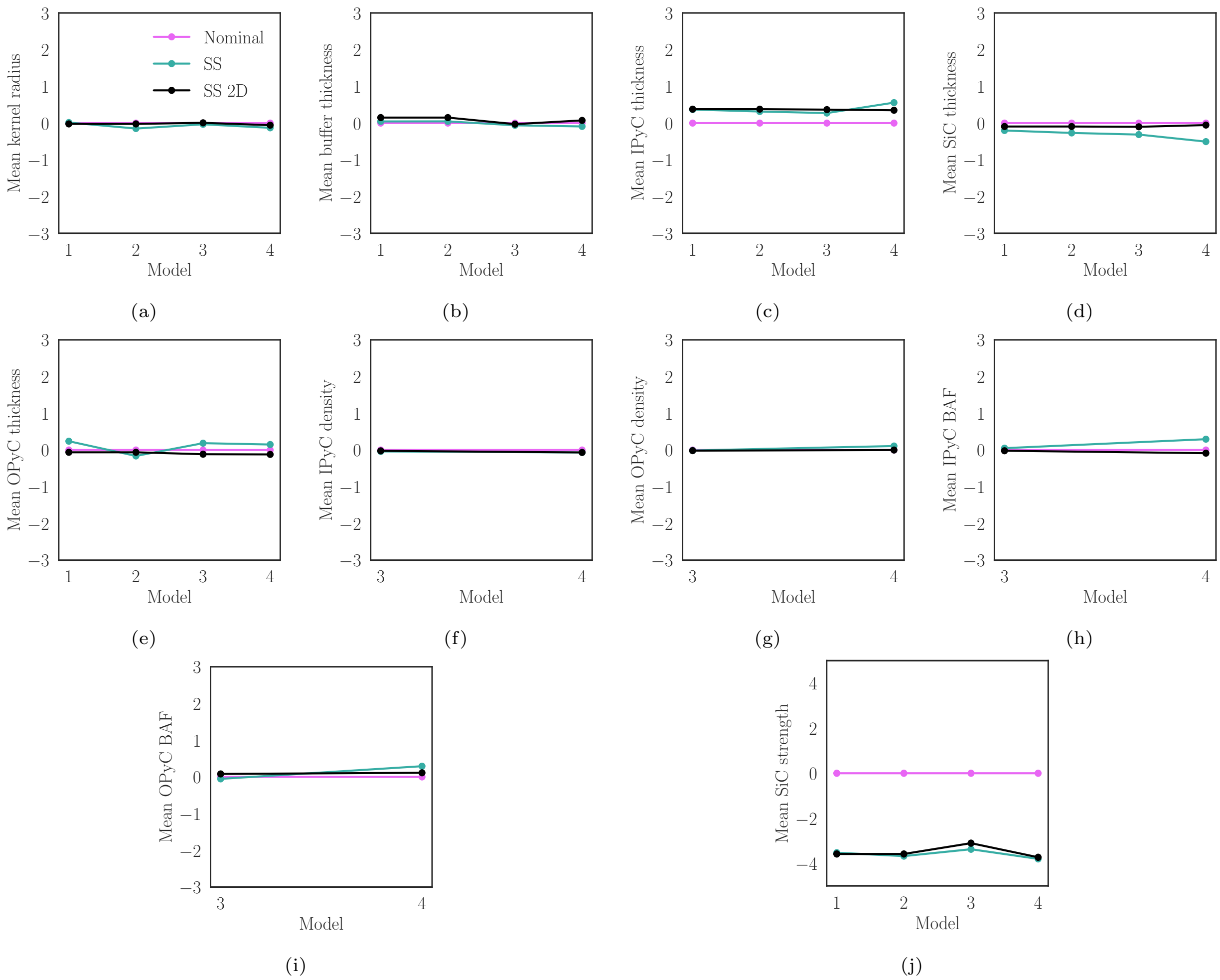


Figure 15: Mean values of the SiC failure-causing input parameters conditional on IPyC failure, computed via SS for all four 2-D and 1-D TRISO models. All distributions are transformed into a standard normal space.

## 6. Discussion on the efficacy of different statistical methods for the failure characterization of nuclear fuels

Several statistical methods were discussed and implemented for failure analysis of nuclear TRISO fuel. The advantages and disadvantages of these methods are assessed here with respect to five characteristics: number of model calls, amenability to parallelization, level of modeling fidelity that can be considered, information on the input parameters that cause model failures, and ability to consider multiple failure modes. Table 6 concisely compares the five methods in terms of these characteristics.

Both MCS and LHS require a very large number of calls to the model, especially when the failure probabilities are low. Variance reduction methods such as AIS and SS require 2–3 orders of magnitude fewer model calls than either MCS or LHS. The Weibull theory requires even fewer model calls than does either AIS or SS (1–2 orders of magnitude fewer). However, the number of model calls should be discussed in combination with the method's amenability for parallelization, and more specifically, the number of model calls per processor. All the methods except the version of AIS presented in this paper can be parallelized. Therefore, the parallel versions of MCS and LHS require a similar number of model calls as AIS, and the parallel SS still requires considerably fewer model calls than parallel MCS or LHS.

Table 6: Capabilities of different statistical methods for the safety assessment of nuclear fuels.

| **Method** | **Model calls**† | **Parallelization** | **Modeling fidelity** | **Input parameter distributions of failed models** | **Multiple failure modes** |
|---|---|---|---|---|---|
| **Standard methods** | | | | | |
| Monte Carlo Sampling (MCS) | $\sim\ 1E6 - 1E7$ | Yes | Low-fidelity | Yes | Yes |
| Latin Hypercube Sampling (LHS) | $\sim\ 1E6 - 1E7$ | Yes | Low-fidelity | Yes | Yes |
| **Variance reduction methods** | | | | | |
| Adaptive Importance Sampling (AIS) | $\sim\ 1E4$ | No | Low-fidelity | Yes‡ | Yes |
| Subset Simulation (SS) | $\sim\ 1E4$ | Yes | Low- and high-fidelity | Yes | Yes |
| **Distribution sampling** | | | | | |
| Weibull Approach (W) | $\sim\ 1E2$ | Yes | Low- and high-fidelity | No | No^ |

† For a target failure probability of $\sim 1E - 4$ and a coefficient of variation of 0.05–0.1
‡ Can potentially be inaccurate due to reliance on a single Markov chain
^ Can be used only when failure is described by the Weibull failure criterion [31]

Even with parallel computing, both MCS and LHS are too computationally prohibitive to be used with high-fidelity fuel models. Therefore, their use is limited to low-fidelity models. Since the AIS version presented in this paper cannot be parallelized, its applicability is also limited to low-fidelity fuel models. Parallel SS and the Weibull theory require fewer model calls per processor and can consider high-fidelity fuel models such as the 2-D TRISO model. Tables 4 and 5 provide more information on the computational times and the number of processors used by the parallel SS and the Weibull theory for 1D and 2D TRISO fuel models.

In principle, all methods except the Weibull theory can characterize the distribution of input parameters that cause model failure. However, with MCS and LHS, when the failure probability is small and the COV is high, a very small set of the simulations indicates failure, which leads to significant uncertainties in these distributions. While AIS can characterize these distributions, the characterizations could be inaccurate, since this method may underexplore the input parameter space, due to its reliance on a single Markov chain. SS relies on multiple Markov chains (on the order of hundreds) and is thus better able to explore the parameter space.

Nuclear fuels can have several interdependent failure modes. For example, TRISO fuel can fail due to tensile stresses in the SiC layer as a result of fission gas buildup in the fuel kernel, stress concentration in the SiC layer as a result of IPyC cracking, debonding between the IPyC and SiC layers [17] (consideration of this failure mode in Bison is under active development), kernel migration [19], and thinning or degradation of the SiC layer [18]. An ideal statistical method would be able to consider multiple interdependent failure modes. MCS, LHS, and AIS rely on generic indicator functions to characterize model failure and can consider interdependent failure modes. SS, while relying directly on the model outputs and not on indicator functions to characterize failure, can also consider interdependent failure modes. Studies such as Hsu and Ching [10], Li et al. [14] describe in greater detail the use of SS with interdependent failure modes. The Weibull method can only be used if the Weibull criterion [31] is used to characterize failure. When failure is not described by the Weibull criterion or when some of the interdependent failure modes do not follow the Weibull criterion, the Weibull method may not be strictly applicable [19].

Apart from the five aspects discussed in Table 6, calculation of fission product release is an important component of nuclear fuel safety analysis [9]. To compute the fraction of fission product release, the time to failure of the fuel and the location of failure [19] must both be known. Standard methods such as MCS and LHS can calculate fission product release but are computationally expensive when used with high-fidelity fuel models. Miller et al. [19] extended the Weibull theory for fission product release by making certain approximations. With respect to the use of AIS and parallel SS, although they are, in principle, capable of calculating fission product release, a future study will investigate this in more detail and compare their accuracies and efficiencies with those of the other methods.

## 7. Summary and conclusions

Failure analysis of nuclear fuel models typically involves numerous model evaluations by varying the uncertain geometric and material parameters of the fuel. Since numerous model evaluations are computationally expensive, low-fidelity fuel models are used for failure analysis. However, it is desirable to use high-fidelity fuel models in view of their improved accuracy, though this further increases the computational expense. This study presented several statistical methods recently implemented in MOOSE (the computational framework underpinning Bison) for failure analysis of nuclear fuels, and applied these methods to TRISO fuel analysis. These methods include standard approaches (i.e., MCS and LHS) as well as alternative approaches (i.e., AIS, SS, and the Weibull theory) that can dramatically accelerate TRISO failure analysis. Among these methods, AIS and SS are classified as variance reduction Monte Carlo methods. Both 1-D and 2-D representations of the four TRISO models were considered, and their results across the different statistical methods were compared in terms of failure probabilities and distributions of input parameters that cause TRISO failure. Based on this study, the efficacy of the different statistical methods was compared with respect to the number of model calls, amenability for parallelization, level of modeling fidelity, input parameter distributions of failed models, and ability to consider multiple failure modes.

The following conclusions can be drawn from this study:

- Under the 1-D representation, all five methods generated similar estimates of failure probabilities for each of the four TRISO models. Importantly, SS and the Weibull theory required about 2–3 orders of magnitude fewer model calls per processor compared to MCS, LHS, and AIS.
- The input parameter distributions of failed TRISO particles obtained using the MCS, LHS, and SS methods were consistent. AIS, while capable of characterizing these distributions, resulted in some inaccuracies due to reliance on a single Markov chain, as well as underexploration of the parameter space. It is infeasable to obtain these parameter distributions using the Weibull theory.
- Because of the relatively high computational cost of the 2-D model, only SS and the Weibull theory were used to analyze failure probabilities of the 2-D models of the four TRISO models. The failure probability estimates generated were consistent between the SS and Weibull methods for the 2-D models.
- While the failure probability estimates were also consistent between the 1-D and 2-D models for spherical particles, the 1-D model led to lesser predicted failure probabilities for the aspherical particles subjected to lower temperatures. These differences can be explained by the approximation quality of the 1-D model stress modification factors and the 2-D model mesh density.
- Because of their ability to directly use high-fidelity fuel models, both the SS and the Weibull theory offer significant benefits for fuel failure analysis. Unlike the Weibull theory, SS can provide information on the input parameters that cause fuel failure, while also considering interdependent failure models that do not follow the Weibull failure criterion.

In addition to fuel failure analysis, calculating fission product release is an important component of nuclear fuel safety analysis. A future study will investigate the efficiency and accuracy of these statistical methods—especially SS and the Weibull theory, given their ability to consider high-fidelity models—for fission product release assessments. From an algorithmic viewpoint, there has been interest in using active learning concepts to perform statistical failure analysis of expensive numerical models. By substituting high-fidelity model outputs with efficient machine learning predictions and calling the computationally expensive model only when required, active learning can considerably reduce the computational expense of statistical failure analysis (by about 2–3 orders of magnitude, compared to SS; see Dhulipala et al. [5]). Application of active learning concepts to nuclear fuel safety assessments will also be explored in the future.


### Acknowledgment

This research is supported through INL's Laboratory Directed Research & Development (LDRD) program under DOE Idaho Operations Office Contract DE-AC07-05ID14517. This research made use of the resources of the High Performance Computing Center at INL, which is supported by the Office of Nuclear Energy of the U.S. DOE and the Nuclear Science User Facilities under Contract No. DE-AC07-05ID14517.


### References


[1] S. K. Au and J. L. Beck. A new adaptive importance sampling scheme for reliability calculations. *Structural Safety*, 21 (2):135–158, 1999. doi: 10.1016/S0167-4730(99)00014-4.

[2] S. K. Au and J. L. Beck. Estimation of small failure probabilities in high dimensions by subset simulation. *Probabilistic engineering mechanics*, 16(4):263–277, 2001. doi: 10.1016/S0266-8920(01)00019-4.

[3] Y. Che, X. Wu, G. Pastore, W. Li, and K. Shirvan. Application of kriging and variational bayesian monte carlo method for improved prediction of doped uo2 fission gas release. *Annals of Nuclear Energy*, 153:108046, 2021. doi: 10.1016/j.anucene.2020.108046.

[4] P. A. Demkowicz, B. Liu, and J. D. Hunn. Coated particle fuel: Historical perspectives and current progress. *Journal of Nuclear Materials*, 515:434–450, 2019. doi: 10.1016/j.jnucmat.2018.09.044.

[5] S. L. N. Dhulipala, M. D. Shields, B. W. Spencer, C. Bolisetti, A. E. Slaughter, V. M. Laboure, and P. Chakroborty. Active learning with multifidelity modeling for efficient rare event simulation, 2021. arXiv:2106.13790.

[6] K.A. Gamble, G. Pastore, M.W.D. Cooper, D.A. Andersson, C. Matthews, B. Beeler, L.K. Aagesen, T. Barani, and D. Pizzocri. Improvement of the bison u3si2 modeling capabilities based on multiscale developments to modeling fission gas behavior. *Journal of Nuclear Materials*, page 153097, 2021. doi: 10.1016/j.jnucmat.2021.153097.

[7] H.D. Gougar, D.A. Petti, P.A. Demkowicz, W.E. Windes, G. Strydom, J.C. Kinsey, J. Ortensi, M. Plummer, W. Skerjanc, R.L. Williamson, and R.N. Wright. The us department of energy's high temperature reactor research and development program–progress as of 2019. *Nuclear Engineering and Design*, 358:110397, 2020. doi: 10.1016/j.nucengdes.2019.110397.

[8] J. D. Hales, R. L. Williamson, S. R. Novascone, D. M. Perez, B. W. Spencer, and G. Pastore. Multidimensional multiphysics simulation of triso particle fuel. *Journal of Nuclear Materials*, 443(1-3):531–543, 2013. doi: 10.1016/j.jnucmat.2013.07.070.

[9] J. D. Hales, W. Jiang, A. Toptan, and K. A. Gamble. Modeling fission product diffusion in triso fuel particles with bison. *Journal of Nuclear Materials*, 548:152840, 2021. doi: 10.1016/j.jnucmat.2021.152840.

[10] W. C. Hsu and J. Ching. Evaluating small failure probabilities of multiple limit states by parallel subset simulation. *Probabilistic Engineering Mechanics*, 25(3):291–304, 2010. doi: 10.1016/j.probengmech.2010.01.003.

[11] W. Jiang, B. W. Spencer, and J. E. Dolbow. Ceramic nuclear fuel fracture modeling with the extended finite element method. *Engineering Fracture Mechanics*, 223:106713, 2020. doi: 10.1016/j.engfracmech.2019.106713.

[12] W. Jiang, Hales J. D., B. W. Spencer, B. P. Collin, A. E. Slaughter, S. R. Novascone, A. Toptan, K. A. Gamble, and R. Gardner. Triso particle fuel performance and failure analysis with bison. *Journal of Nuclear Materials*, 548:152795, 2021. doi: j.jnucmat.2021.152795.

[13] H. S. Li and Z. J. Cao. Matlab codes of subset simulation for reliability analysis and structural optimization. *Structural and Multidisciplinary Optimization*, 54(2):391–410, 2016. doi: 10.1007/s00158-016-1414-5.

[14] H. S. Li, Y. Z. Ma, and Z. Cao. A generalized subset simulation approach for estimating small failure probabilities of multiple stochastic responses. *Computers & Structures*, 153:239–251, 2015. doi: 10.1016/j.compstruc.2014.10.014.

[15] M.D. McKay, R.J. Beckman, and W.J. Conover. A comparison of three methods for selecting values of input variables in the analysis of output from a computer code. *Technometrics*, 21(2):239–245, 1979. doi: 10.2307/1268522.

[16] R. E. Melchers and A. T. Beck. *Structural reliability analysis and prediction.* John wiley & sons, 2017. doi: 10.1002/9781119266105.

[17] G. K. Miller, D. A. Petti, and J. T. Maki. Consideration of the effects of partial debonding of the ipyc and particle asphericity on triso-coated fuel behavior. *Journal of Nuclear Materials*, 334(2-3):79–89, 2004. doi: j.jnucmat.2004.04.330.

[18] G. K. Miller, D. A. Petti, J. T. Maki, and D. L. Knudson. An evaluation of the effects of sic layer thinning on failure of triso-coated fuel particles. *Journal of Nuclear Materials*, 355(1-3):150–162, 2006. doi: 10.1016/j.jnucmat.2006.05.016.

[19] G. K. Miller, D. A. Petti, J. T. Maki, D. L. Knudson, and W. F. Skerjanc. *PARFUME Theory and Model Basis Report (No. INL/EXT-08-14497-Rev001).* Idaho National Lab, Idaho Falls, ID, USA, 2018. doi: 10.2172/1471713.

[20] J. Morio and M. Balesdent. *Estimation of rare event probabilities in complex aerospace and other systems: a practical approach.* Elsevier-Woodhead Publishing, Sawston, United Kingdom, 2015. doi: 10.1016/C2014-0-02344-1.

[21] A. Olsson, G. Sandberg, and O. Dahlblom. On latin hypercube sampling for structural reliability analysis. *Structural Safety*, 25(1):47–68, 2003. doi: 10.1016/S0167-4730(02)00039-5.

[22] K. M. Paaren, N. Lybeck, K. Mo, P. Medvedev, and D. Porter. Cladding profilometry analysis of experimental breeder reactor-ii metallic fuel pins with ht9, d9, and ss316 cladding. *Energies*, 14(2):515, 2021. doi: 10.3390/en14020515.

[23] C. Parisi, Z. Ma, D. Mandelli, N. Anderson, and H. Zhang. Risk-informed safety analysis for accident tolerant fuels. *Nuclear Science and Engineering*, 194(8-9):748–770, 2020. doi: 10.1080/00295639.2020.1732699.

[24] C.J. Permann, D.R. Gaston, D. Andrs, R.W. Carlsen, F. Kong, A.D. Lindsay, J.M. Miller, J.W. Peterson, A.E. Slaughter, R.H. Stogner, and R.C. Martineau. Moose: Enabling massively parallel multiphysics simulation. *SoftwareX*, 11:100430, 2020. doi: 10.1016/j.softx.2020.100430.

[25] R. Y. Rubinstein and D. P. Kroese. *Simulation and the Monte Carlo method (Vol. 10)*. John Wiley & Sons, Hoboken, NJ, USA, 2016. doi: 10.1002/9781118631980.

[26] M. D. Shields and J. Zhang. The generalization of latin hypercube sampling. *Reliability Engineering & System Safety*, 148:96–108, 2016. doi: 10.1016/j.ress.2015.12.002.

[27] M. D. Shields, D. G. Giovanis, and V. S. Sundar. Subset simulation for problems with strongly non-gaussian, highly anisotropic, and degenerate distributions. *Computers & Structures*, 245:106431, 2021. doi: 10.1016/j.compstruc.2020.106431.

[28] W. F. Skerjanc, J. T. Maki, B. P. Collin, and D. A. Petti. Evaluation of design parameters for triso-coated fuel particles to establish manufacturing critical limits using parfume. *Journal of Nuclear Materials*, 469:99–105, 2016. doi: 10.1016/j.jnucmat.2015.11.027.

[29] R. L. Williamson, J. D. Hales, S. R. Novascone, M. R. Tonks, D. R. Gaston, C. J. Permann, D. Andrs, and R.C. Martineau. Multidimensional multiphysics simulation of nuclear fuel behavior. *Journal of Nuclear Materials*, 423(1):149–163, 2012. doi: 10.1016/j.jnucmat.2012.01.012.

[30] R. L. Williamson, J. D. Hales, S. R. Novascone, G. Pastore, K. A. Gamble, B. W. Spencer, W. Jiang, S. A. Pitts, A. Casagranda, D. Schwen, A. X. Zabriskie, A. Toptan, R. Gardner, C. Matthews, W. Liu, and H. Chen. Bison: A flexible code for advanced simulation of the performance of multiple nuclear fuel forms. *Nuclear Technology*, 207(7):954–980, 2021. doi: 10.1080/00295450.2020.1836940.

[31] F. W. Zok. On weakest link theory and Weibull statistics. *Journal of the American Ceramic Society*, 100(4):1265–1268, 2017. doi: 10.1111/jace.14665.